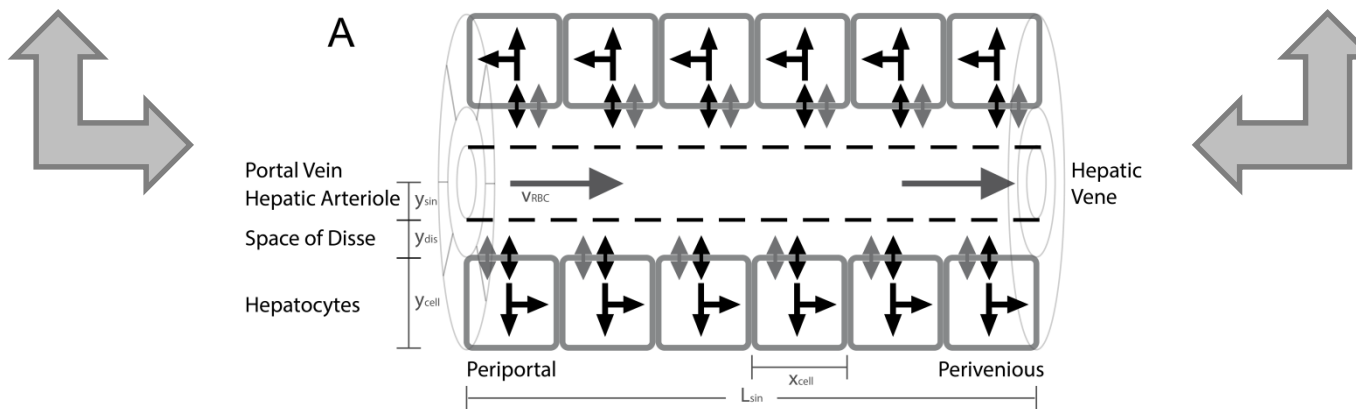
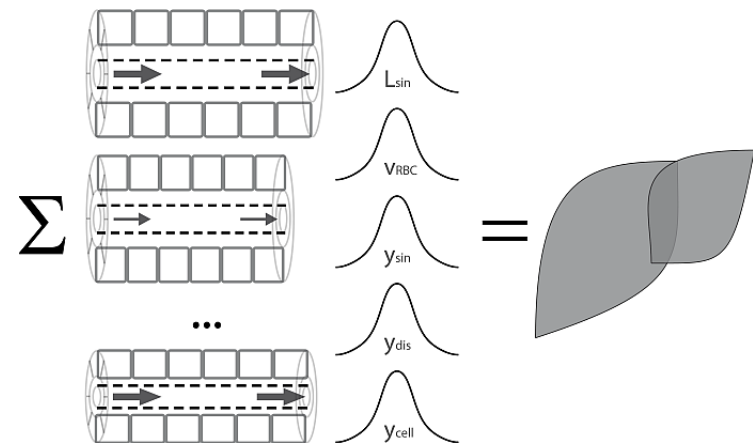
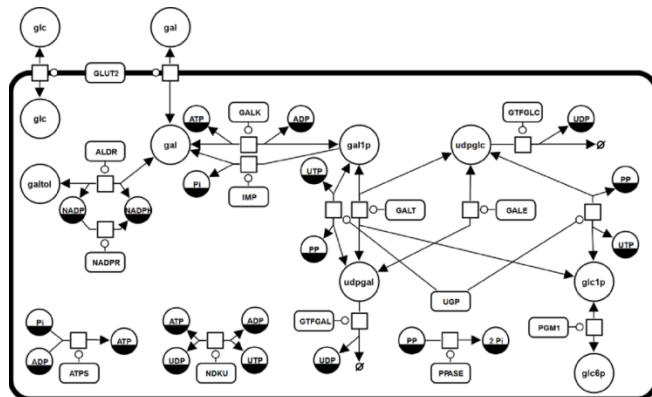
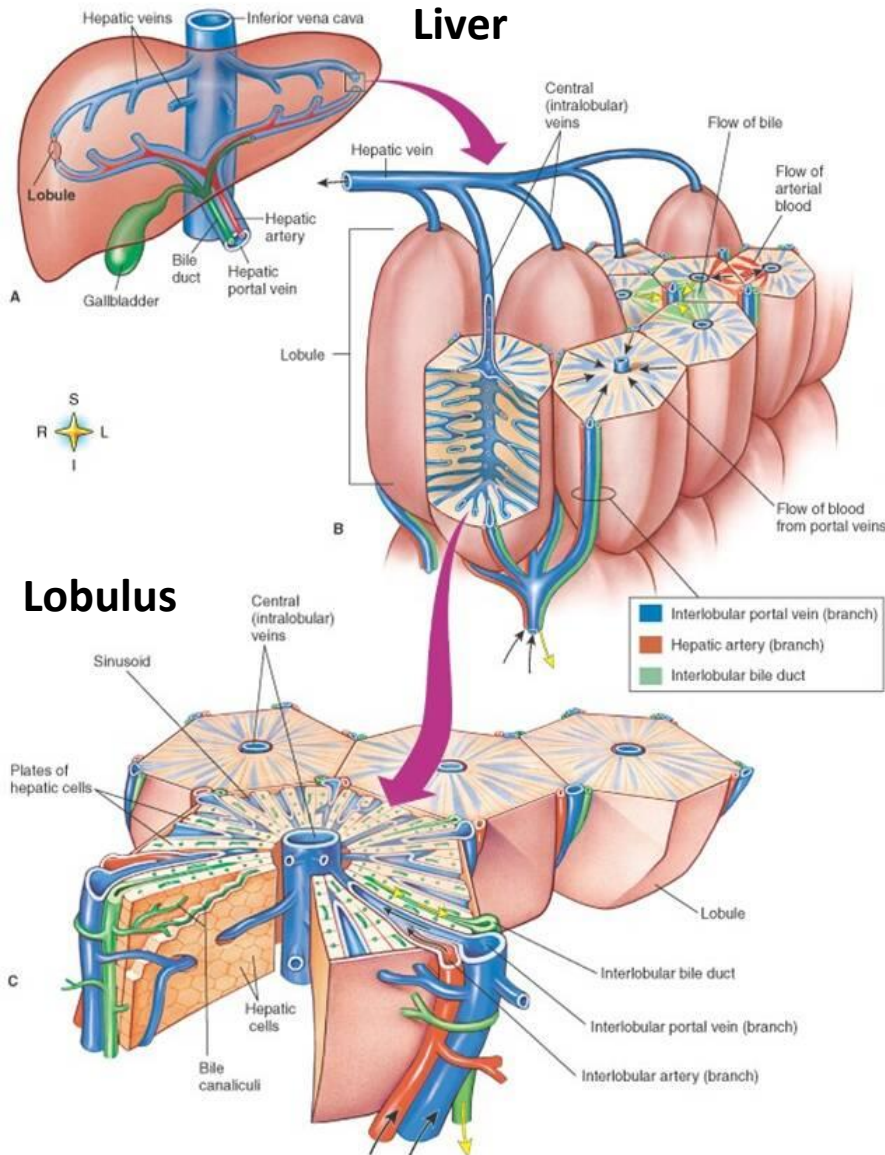


From Hepatocytes to Whole Liver Function: A Multi-scale Model of Human Galactose Metabolism - Sampling Parameter Distributions

König M. & Holzhütter HG.



LIVER ARCHITECTURE

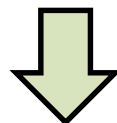


- liver structured in parallel subunits (**liver lobule**)
- liver lobulus consists of **network of sinusoids** connecting hepatic artery and portal vein with the **central vein (periportal → perivenous)**



Tissue parameter distributions

- Fit distributions to experimental data

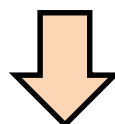


Sampling Sinusoidal Unit Architectures

- LHS
- Distribution
- Mixed

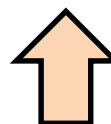
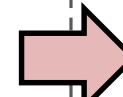
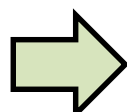
Algorithm

- Method (ODE, SS, MCA)
- Parameters (tolerances, stepsize,...)



Simulation

- C++



Single Cell Model

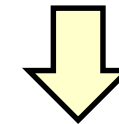
- Fit Vmax to experimental data
- Initialization (i.e. Galactosemias)

Timecourse Events

- Define changes in boundary conditions (peaks, parameters changes, ...)

Database storage

- Store models, algorithms, samplings, events, timecourses (CSV)
- Reproducibility
- Simplify data analysis

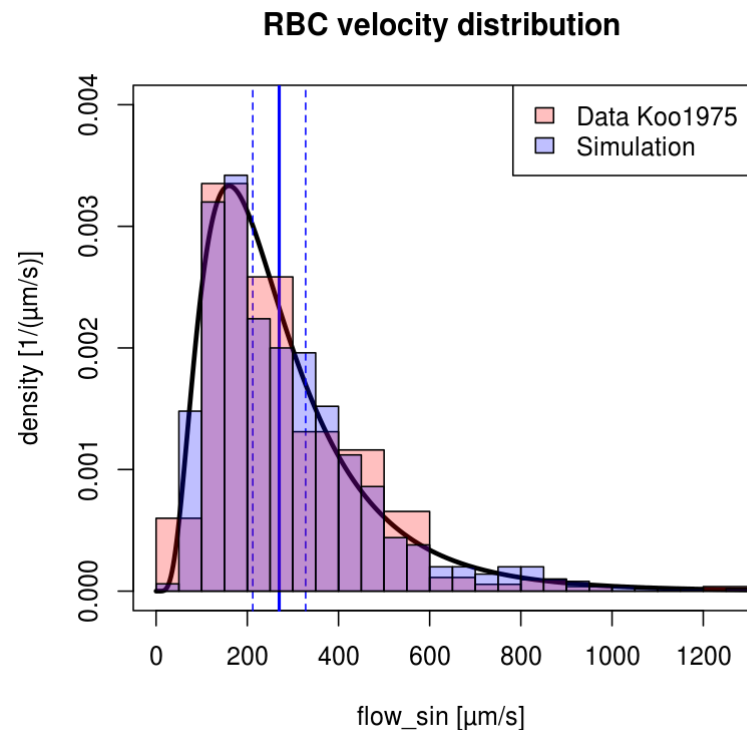
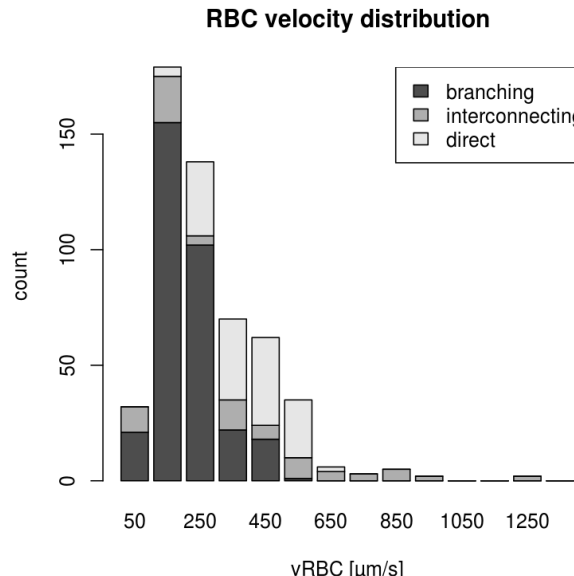


Postprocessing & Analysis

- Probability-weighted averaging
- Scaling from samples to whole liver
- Generate figures

FITTING DISTRIBUTIONS

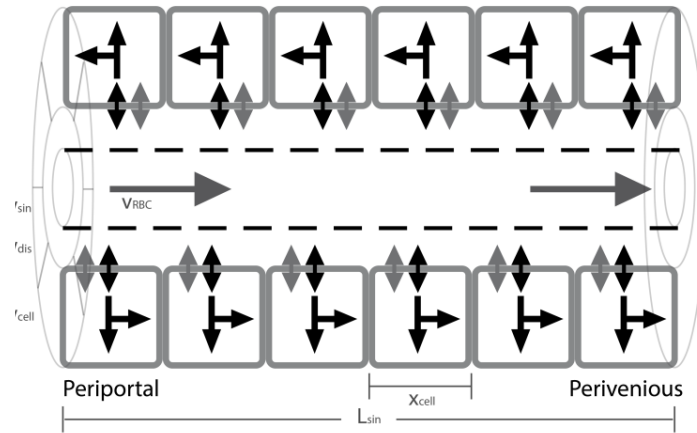
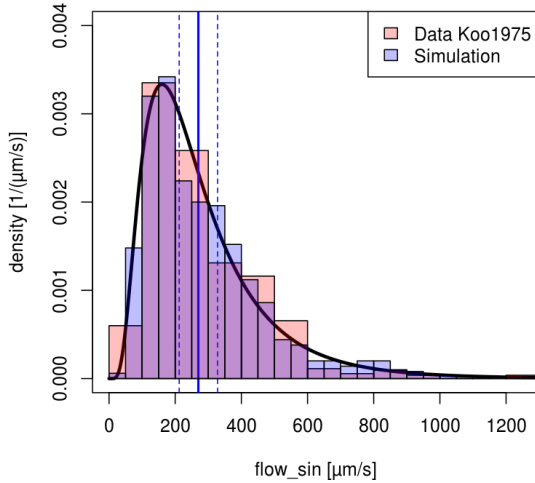
- maximum-likelihood method for univariate distributions (log-normal)



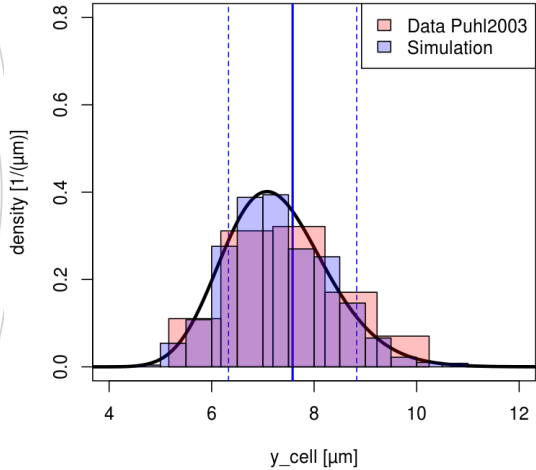
Parameter	meanlog	stdlog	mean μ (reported)	standard deviation (reported)	SD	references
Sinusoidal length	L_{\sin}	6.184	0.2462	500 μm	125 μm	based on distance between central veins 809±199 μm (SD, n=79, young rat, SEM of corrosion cast) (Warren, et al., 2008) scaled to human sinusoidal length
Sinusoidal radius	y_{\sin}	1.465 (± 0.010)	0.1017 (± 0.0073)	4.4 μm	0.45 μm	Based on distribution of sinusoidal diameter 8.8±0.9 μm (SD, n=440 in N=11 human, OPS) (Puhl, et al., 2003)
Width of Disse space	y_{dis}	0.1296	0.3246	1.2 μm	0.4 μm	0.4–1.5 μm (human, SEM, estimated from imaged) (Muto, et al., 1977) 0.5–1.2 μm (human, SEM, estimated from image) (Burwen, et al., 1982) 7.58 μm
Hepatocyte sheet thickness	y_{cell}	1.977 (± 0.014)	0.1390 (± 0.0099)	7.58 μm	1.25 μm	Calculated from functional sinusoidal density FSD FSD 391±30 [1/cm] (SD, n=88, human, OPS) (Puhl, et al., 2003)

TISSUE-SCALE SINUSOIDAL UNIT

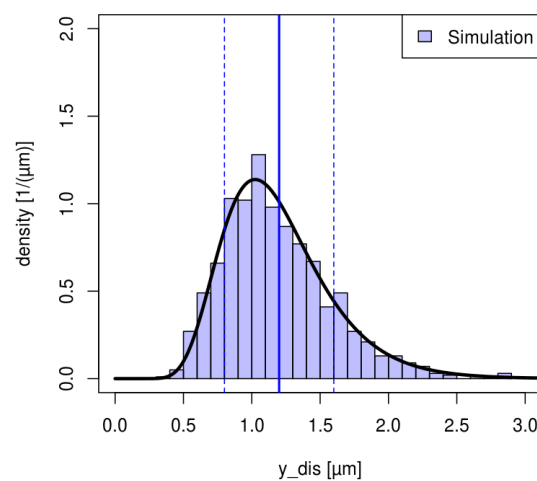
RBC velocity distribution



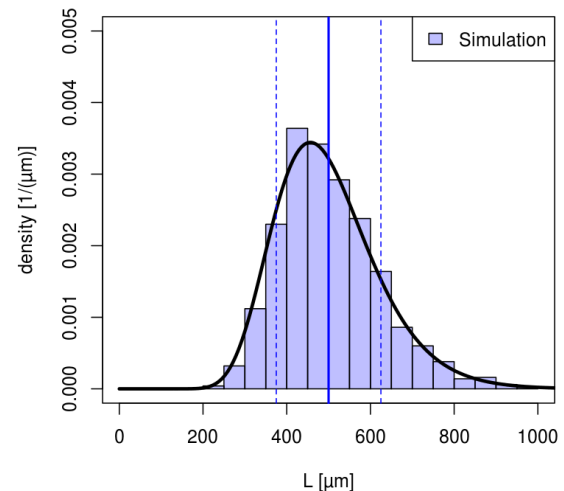
y_{cell} distribution



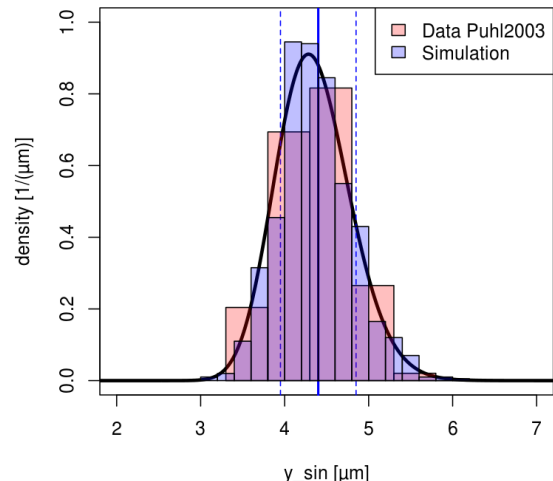
Width space of Disse



Sinusoidal length

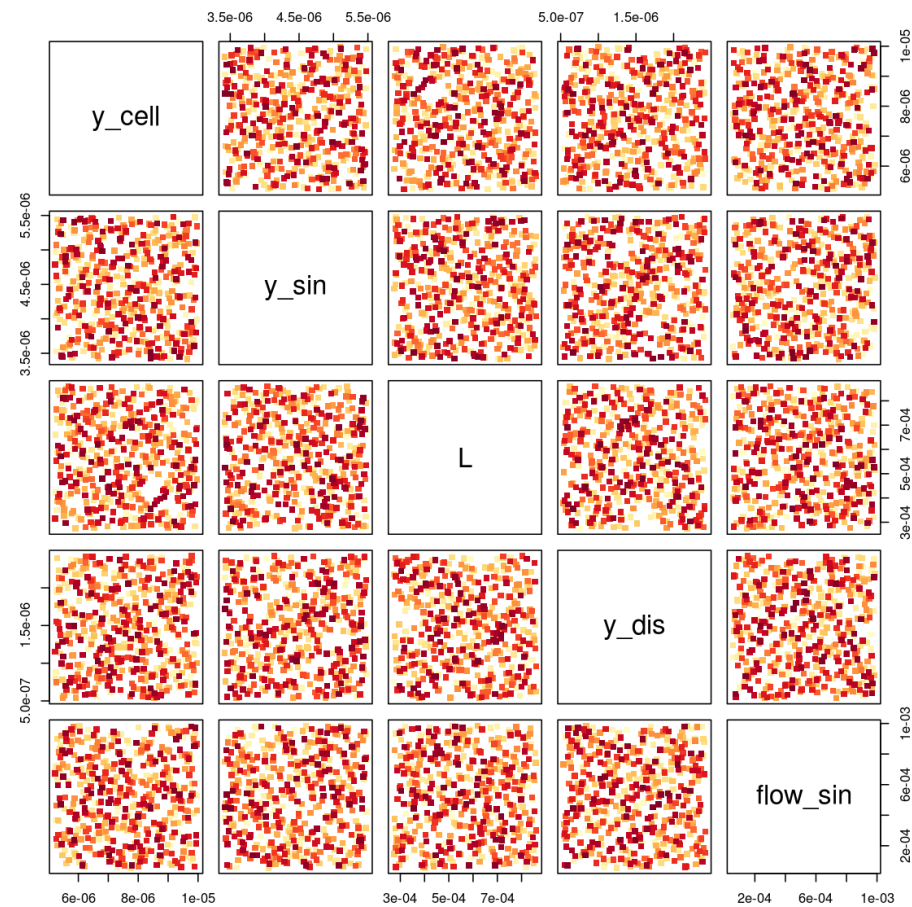
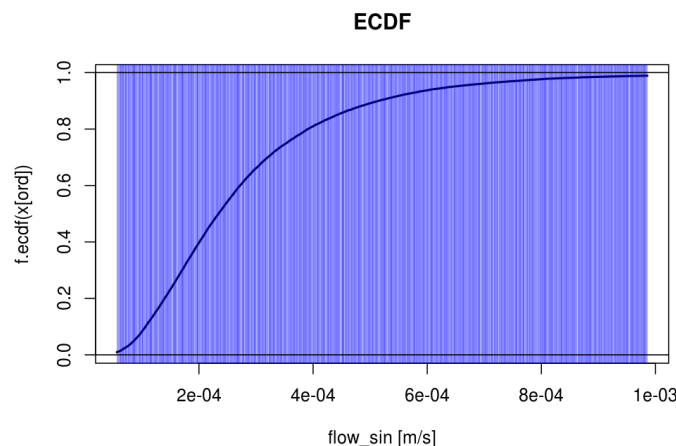
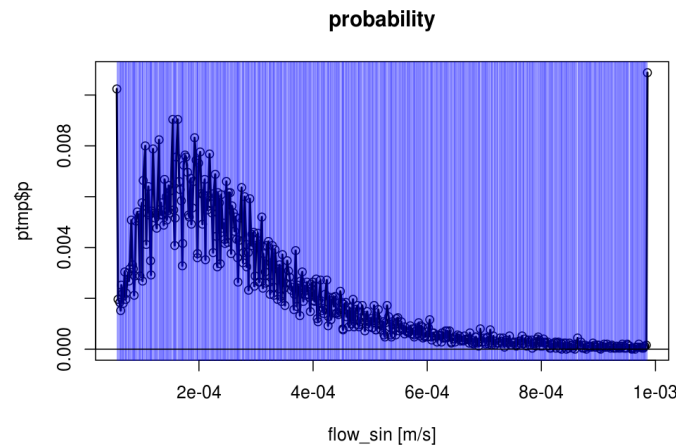


Sinusoidal radius

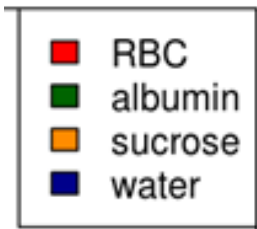


LHS SAMPLING

- Latin hypercube sampling (LHS) & Methods from MonteCarlo sampling

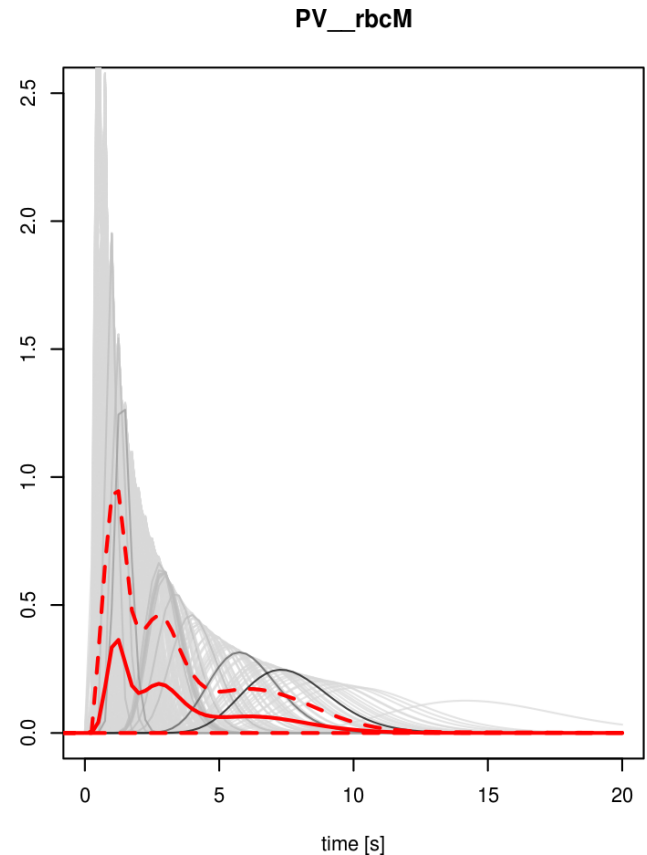
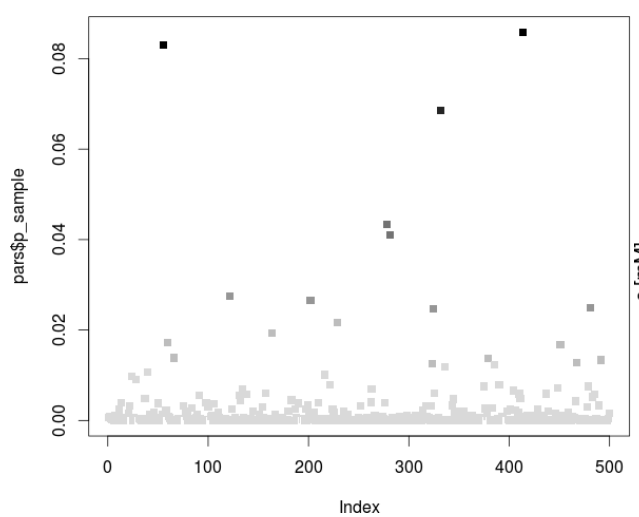
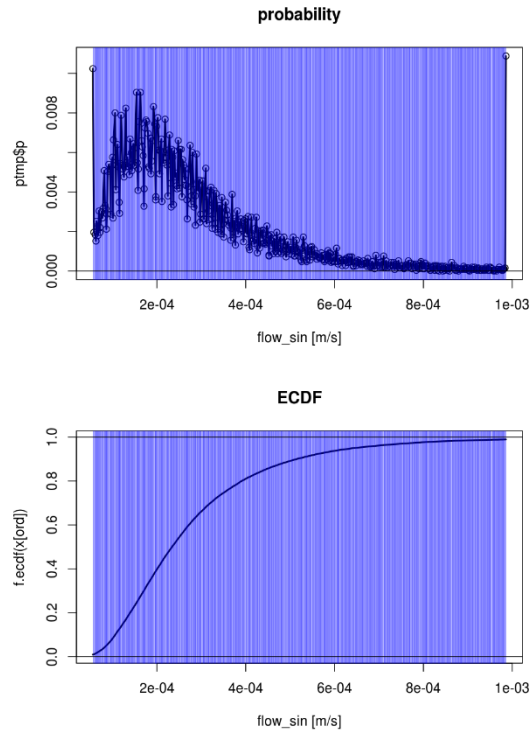


CONVERGENCE



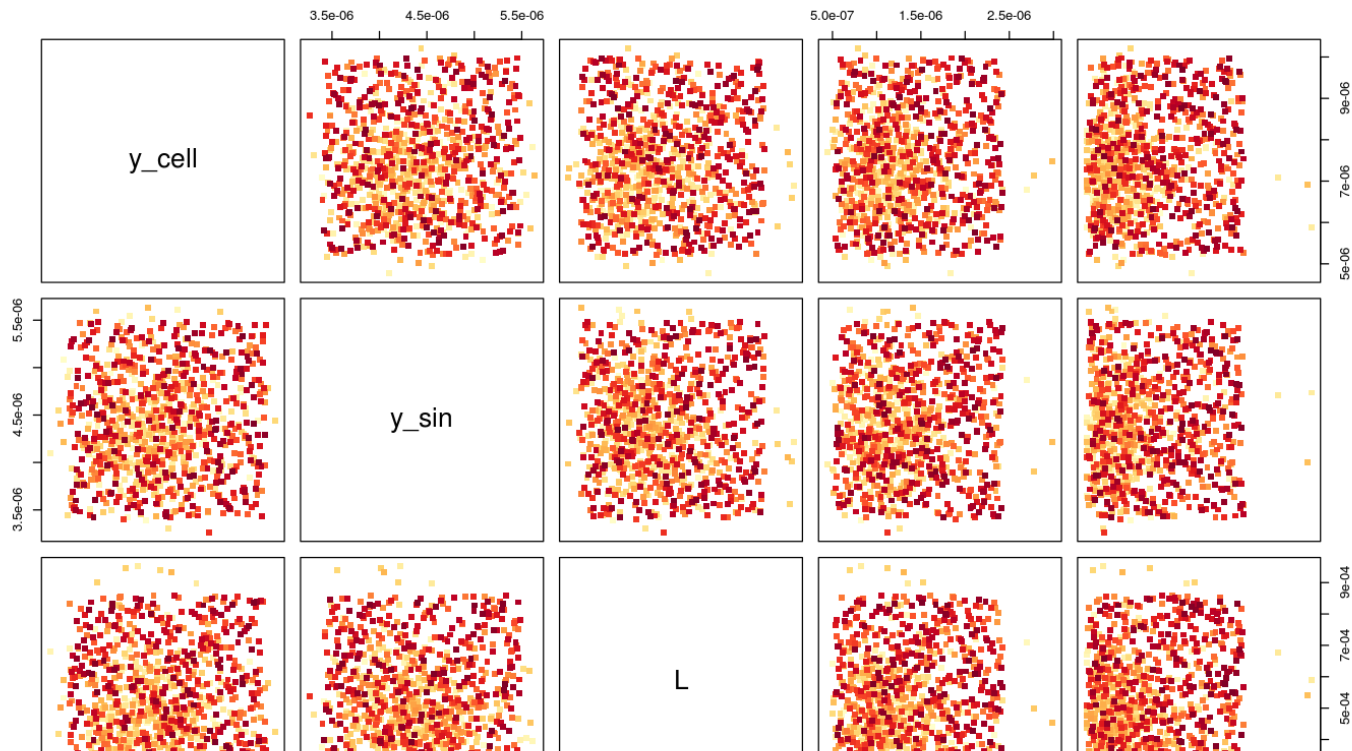
Challenge:

- High-dimensional parameter space (5-10 dimensions in tissue & metabolic parameters)
- Many „clever“ samples necessary to cover space properly



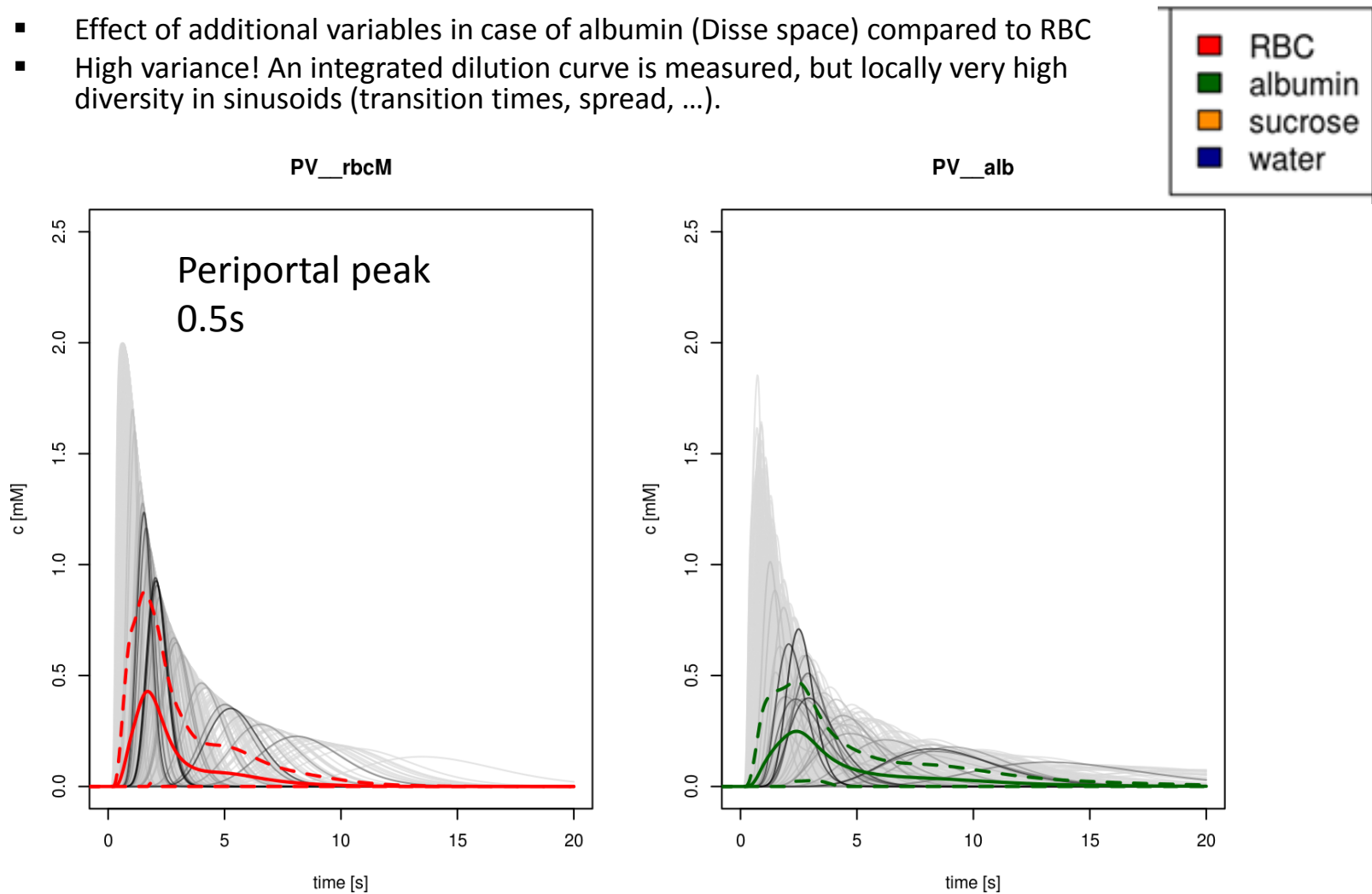
COMBINATION STRATEGY

- **50% LHS** (cover full range from 0.01-0.99 quantiles)
- **50% distribution sampling** (account for highly probable events)
- **ECDF based weighting** (empirical cumulative distribution function) of sample contribution under assumption of statistical independence of parameters



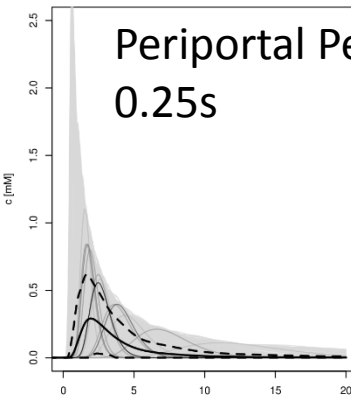
PERIVENIOUS DILUTION CURVES

- Better, but still not optimal
 - N=1000 mixed (500 LHS & 500 distribution) + probability weighting
 - TODO: Drop the statistical independence & construct a multidimensional ECDF
- Note:
 - Effect of additional variables in case of albumin (Disse space) compared to RBC
 - High variance! An integrated dilution curve is measured, but locally very high diversity in sinusoids (transition times, spread, ...).

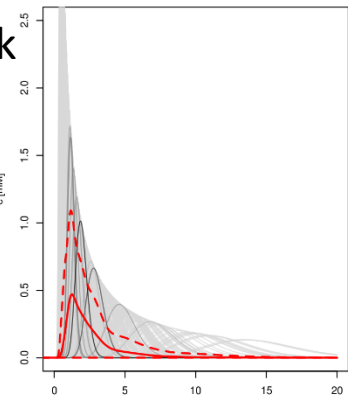


PV_gal

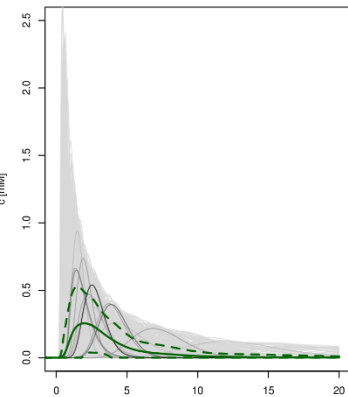
Periportal Peak
0.25s



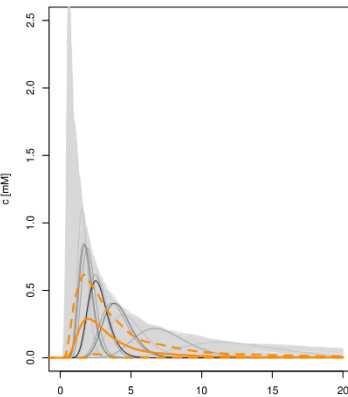
PV_rbcM



PV_alb



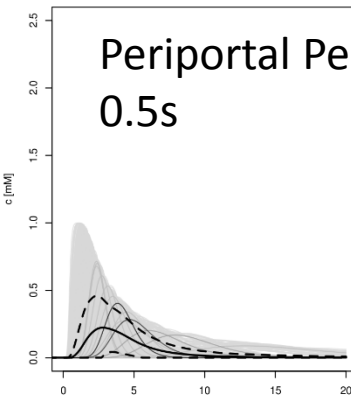
PV_suc



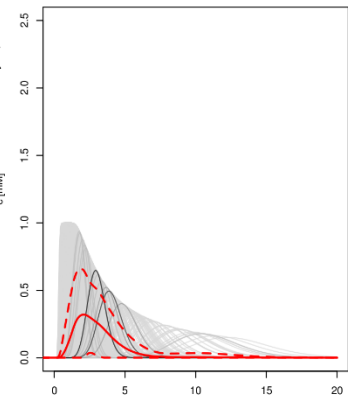
- RBC
- albumin
- sucrose
- water

PV_gal

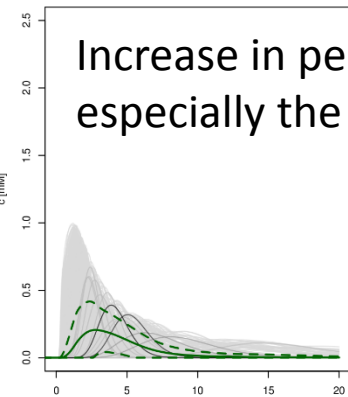
Periportal Peak
0.5s



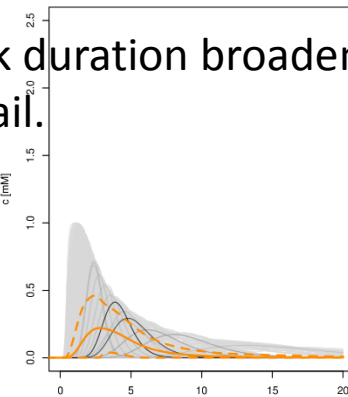
PV_rbcM



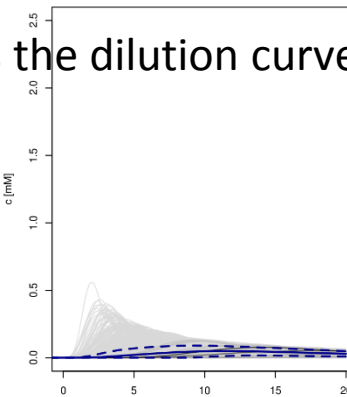
PV_alb



PV_suc



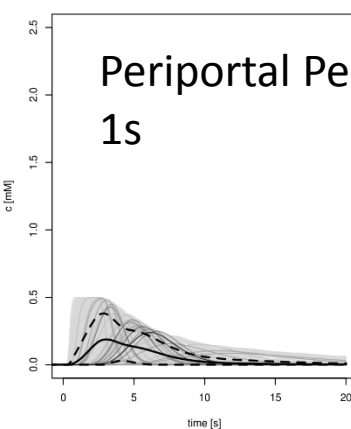
PV_h2oM



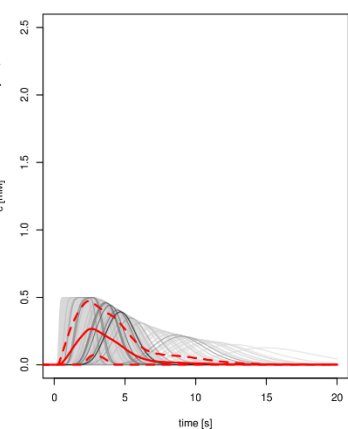
Increase in peak duration broadens the dilution curve, especially the tail.

PV_gal

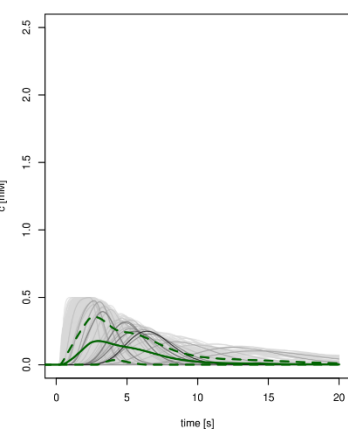
Periportal Peak
1s



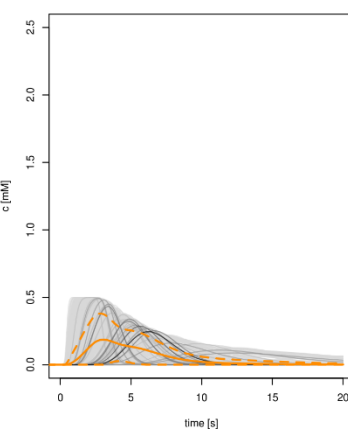
PV_rbcM



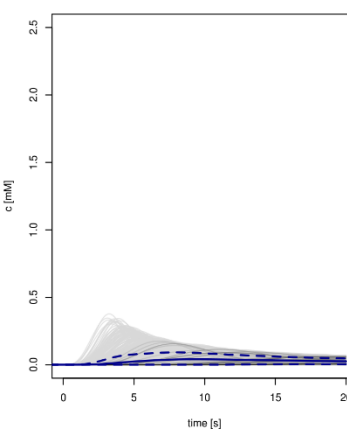
PV_alb



PV_suc



PV_h2oM

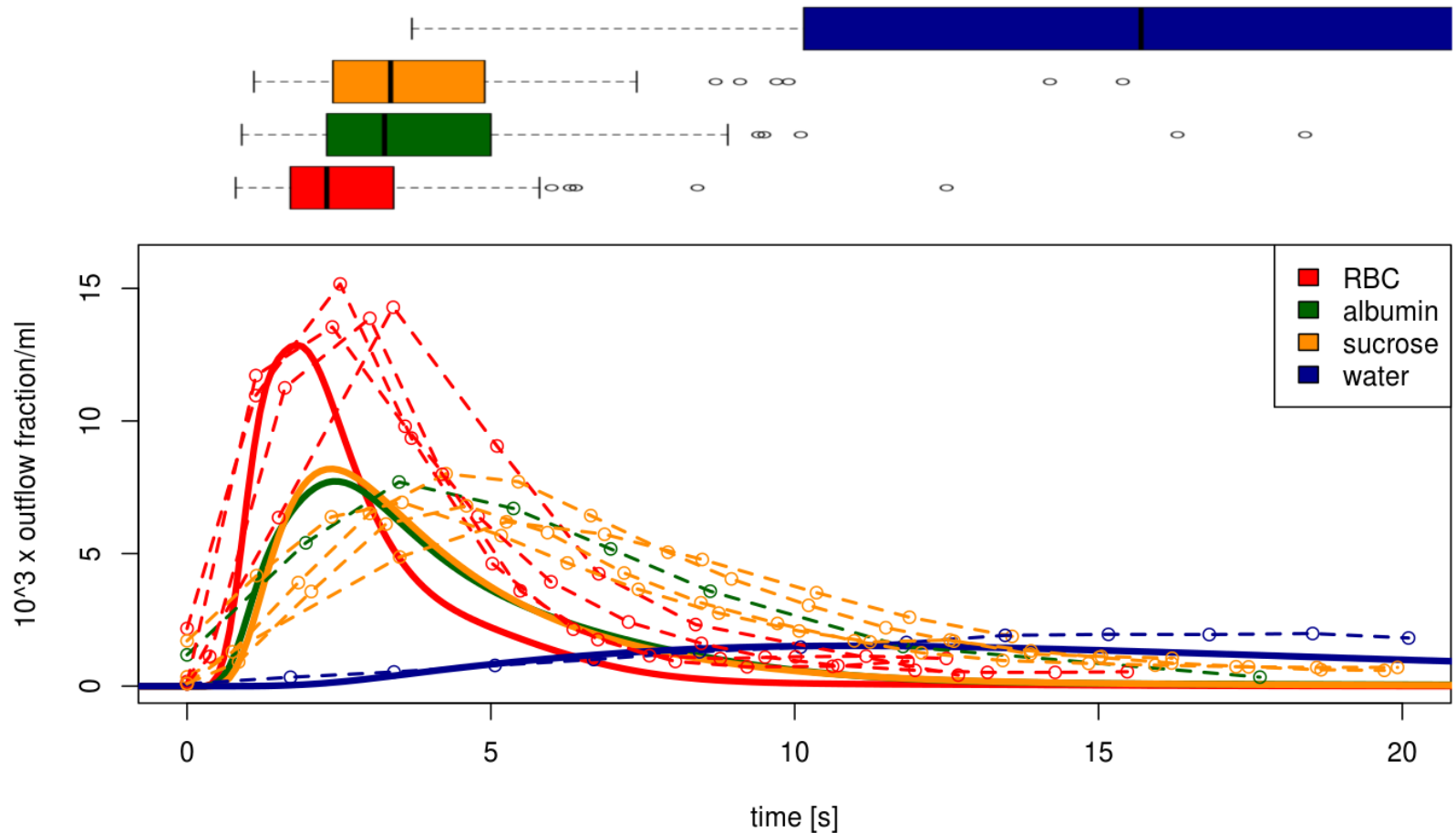


MULTIPLE INDICATOR DILUTION

Mean dilution curves with experimental data from 4 independent experiments

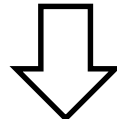
Periportal Peak (rectangular, duration 0.5s)

No fitting (only free parameter is peak duration).



Tissue parameter distributions

- Fit distributions to experimental data

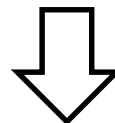


Sampling Sinusoidal Unit Architectures

- LHS
- Distribution
- Mixed

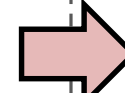
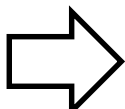
Algorithm

- Method (ODE, SS, MCA)
- Parameters (tolerances, stepsize,...)



Simulation

- C++



Single Cell Model

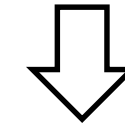
- Fit Vmax to experimental data
- Initialization (i.e. Galactosemias)

Timecourse Events

- Define changes in boundary conditions (peaks, parameters changes, ...)

Database storage

- Store models, algorithms, samplings, events, timecourses (CSV)
- Reproducibility
- Simplify data analysis



Postprocessing & Analysis

- Probability-weighted averaging
- Scaling from samples to whole liver
- Generate figures

Tasks

Models
Tasks
Integrations
Cores
Simulations
Timecourses
Plots

Admin

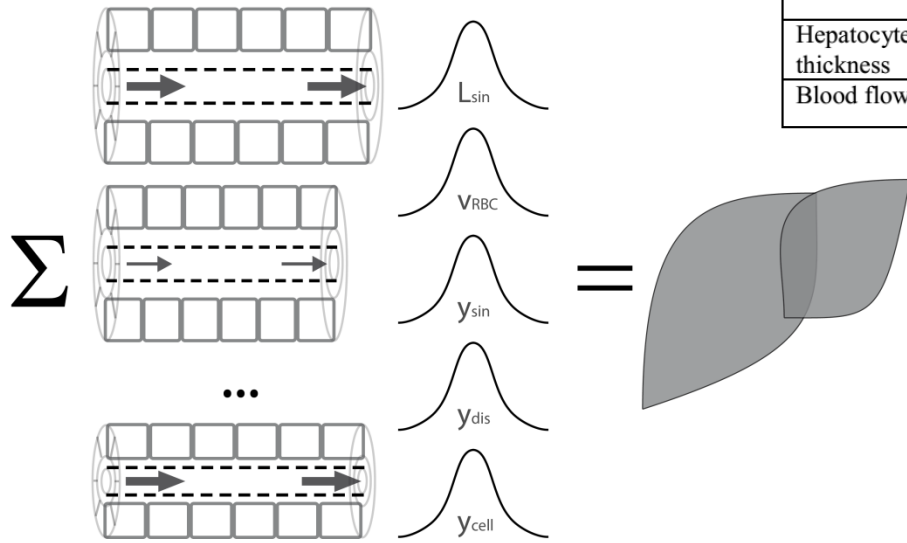


pk	model	integration	simulations	status	info
25	MultipleIndicator_P04_v14_Nc20_Nf1	[0,0.100,0] 4000	1000	1000 0 0	Simulation of multiple-indicator dilution curves (tracer peak periportal)
24	MultipleIndicator_P03_v14_Nc20_Nf1	[0,0.100,0] 4000	1000	1000 0 0	Simulation of multiple-indicator dilution curves (tracer peak periportal)
23	MultipleIndicator_P02_v14_Nc20_Nf1	[0,0.100,0] 4000	1000	1000 0 0	Simulation of multiple-indicator dilution curves (tracer peak periportal)
22	MultipleIndicator_P01_v14_Nc20_Nf1	[0,0.100,0] 4000	1000	1000 0 0	Simulation of multiple-indicator dilution curves (tracer peak periportal)
21	MultipleIndicator_P00_v14_Nc20_Nf1	[0,0.100,0] 4000	1000	1000 0 0	Simulation of multiple-indicator dilution curves (tracer peak periportal)
20	MultipleIndicator_P04_v14_Nc20_Nf1	[0,0.500,0] 2000	1000	1000 0 0	Simulation of multiple-indicator dilution curves (tracer peak periportal)
19	MultipleIndicator_P03_v14_Nc20_Nf1	[0,0.500,0] 2000	1000	1000 0 0	Simulation of multiple-indicator dilution curves (tracer peak periportal)
18	MultipleIndicator_P02_v14_Nc20_Nf1	[0,0.500,0] 2000	1000	1000 0 0	Simulation of multiple-indicator dilution curves (tracer peak periportal)
17	MultipleIndicator_P01_v14_Nc20_Nf1	[0,0.500,0] 2000	1000	1000 0 0	Simulation of multiple-indicator dilution curves (tracer peak periportal)
16	MultipleIndicator_P00_v14_Nc20_Nf1	[0,0.500,0] 2000	1000	1000 0 0	Simulation of multiple-indicator dilution curves (tracer peak periportal)
15	MultipleIndicator_P04_v13_Nc20_Nf1	[0,0.500,0] 2000	500	500 0 0	Simulation of tracer peak periportal with resulting dilution curves.
14	MultipleIndicator_P03_v13_Nc20_Nf1	[0,0.500,0] 2000	500	500 0 0	Simulation of tracer peak periportal with resulting dilution curves.
13	MultipleIndicator_P02_v13_Nc20_Nf1	[0,0.500,0] 2000	500	500 0 0	Simulation of tracer peak periportal with resulting dilution curves.
12	MultipleIndicator_P01_v13_Nc20_Nf1	[0,0.500,0] 2000	500	500 0 0	Simulation of tracer peak periportal with resulting dilution curves.
11	MultipleIndicator_P00_v13_Nc20_Nf1	[0,0.500,0] 2000	500	500 0 0	Simulation of tracer peak periportal with resulting dilution curves.
10	MultipleIndicator_P04_v11_Nc20_Nf1	[0,0.500,0] 2000	1000	1000 0 0	Simulation of tracer peak periportal with resulting dilution curves.
9	MultipleIndicator_P03_v11_Nc20_Nf1	[0,0.500,0] 2000	1000	1000 0 0	Simulation of tracer peak periportal with resulting dilution curves.
8	MultipleIndicator_P02_v11_Nc20_Nf1	[0,0.500,0] 2000	1000	1000 0 0	Simulation of tracer peak periportal with resulting dilution curves.
7	MultipleIndicator_P01_v11_Nc20_Nf1	[0,0.500,0] 2000	1000	1000 0 0	Simulation of tracer peak periportal with resulting dilution curves.
6	MultipleIndicator_P00_v11_Nc20_Nf1	[0,0.500,0] 2000	1000	1000 0 0	Simulation of tracer peak periportal with resulting dilution curves.
5	MultipleIndicator_P04_v10_Nc20_Nf1	[0,0.500,0] 2000	1000	1000 0 0	Simulation of tracer peak periportal with resulting dilution curves.
4	MultipleIndicator_P03_v10_Nc20_Nf1	[0,0.500,0] 2000	1000	1000 0 0	Simulation of tracer peak periportal with resulting dilution curves.
3	MultipleIndicator_P02_v10_Nc20_Nf1	[0,0.500,0] 2000	1000	1000 0 0	Simulation of tracer peak periportal with resulting dilution curves.
2	MultipleIndicator_P01_v10_Nc20_Nf1	[0,0.500,0] 2000	1000	1000 0 0	Simulation of tracer peak periportal with resulting dilution curves.
1	MultipleIndicator_P00_v10_Nc20_Nf1	[0,0.500,0] 2000	1000	1000 0 0	Simulation of tracer peak periportal with resulting dilution curves.

A	B	C	D	E	F	G	H	I	
1	status	core	y_cell	y_sin	L	y_dis	flow_sin	duration	sim
2	UNASSIGNED		6.64640464768893E-006	4.51517526406004E-006	0.0004561854	1.32136941126338E-006	0.000211178		18777
3	UNASSIGNED		8.65649669544174E-006	4.209316151364485E-006	0.0003531316	1.2242684723271E-006	9.00117286863366E-005		18776
4	ASSIGNED	10.39.34.27-cpu-7	0.000009368	4.21789594644714E-006	0.000303369	0.000001333	0.0002640036		18771
5	UNASSIGNED		7.806510890555E-006	3.7518369501097E-006	0.0004087027	7.44808383741511E-007	0.0001856388		18775
6	UNASSIGNED		6.56829981417262E-006	4.66838593564891E-006	0.0004450632	2.18105301284341E-006	0.0005594039		18774
7	UNASSIGNED		0.000007654	0.000004767	0.0004678695	1.28922128018918E-006	0.0006329357		18773
8	UNASSIGNED		6.16586931252047E-006	4.00557810337901E-006	0.0003860545	0.000002106	0.0003230328		18772
9	ASSIGNED	10.39.32.106-cpu-6	0.000006985	4.79876060470051E-006	0.0003815726	1.35365610180616E-006	0.0003462197		18770
10	ASSIGNED	10.39.32.106-cpu-2	7.64105547110986E-006	3.68658262867564E-006	0.0007089434	7.28091402600155E-007	0.0003975799		18769
11	ASSIGNED	10.39.32.106-cpu-3	5.48665402151281E-006	3.94156223503503E-006	0.0007403251	9.94301691554614E-007	0.0002118681		18768
12	DONE	10.39.32.106-cpu-3	7.51433734943539E-006	4.11137911122231E-006	0.0004835724	1.24009474604172E-006	0.0001130779	0:00:16.452447	18659
13	ASSIGNED	10.39.32.106-cpu-4	5.85964337540257E-006	4.98019213658844E-006	0.0005390215	1.10575700208949E-006	0.0004644926		18767
14	DONE	10.39.32.106-cpu-4	7.9036707368155E-006	3.8512395197718E-006	0.0004908441	9.42578939441774E-007	0.0001496508	0:00:19.849417	18654
15	UNASSIGNED		0.00000727	4.39158492126421E-006	0.0004649256	1.16989698017536E-006	0.0002237426		18766
16	UNASSIGNED		6.95890891772681E-006	4.89525231602892E-006	0.0005050888	0.000000766	0.0002073985		18765
17	UNASSIGNED		7.31786542779174E-006	4.33173985805061E-006	0.0004992128	9.06754602912661E-007	0.0001574594		18764
18	UNASSIGNED		6.95367709886474E-006	4.60523088829777E-006	0.0004184891	1.25009968194451E-006	9.28409181927323E-005		18763

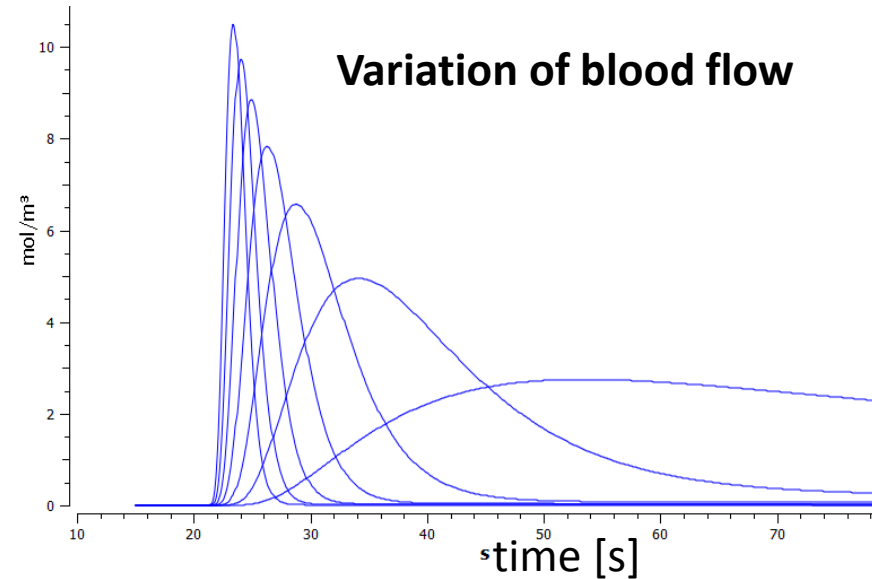
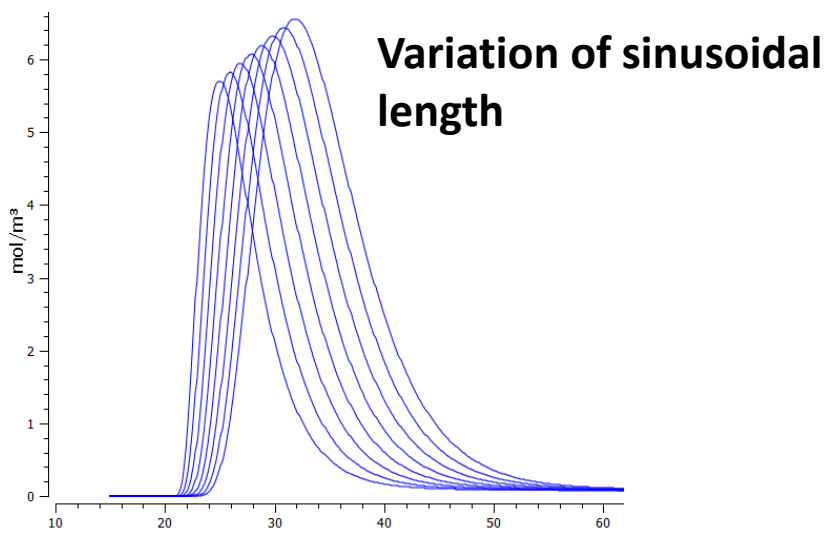
ORGAN-SCALE – WHOLE LIVER METABOLISM

ORGAN-SCALE

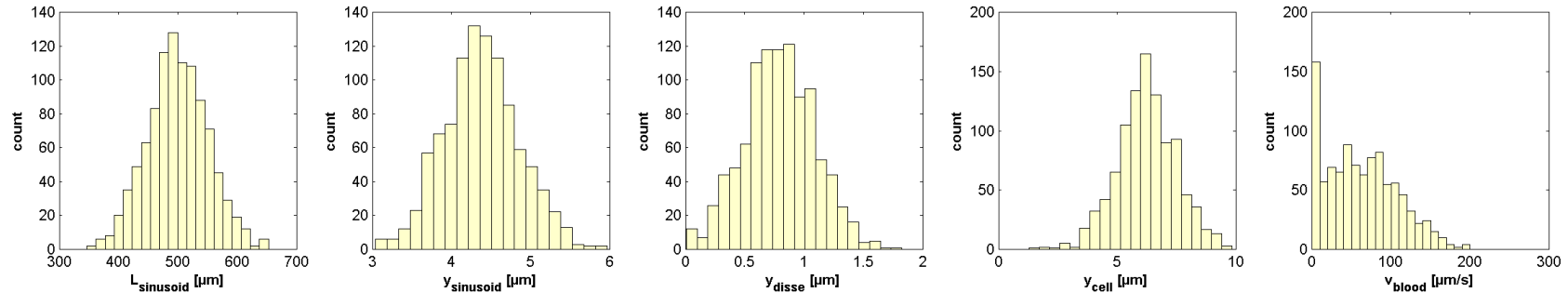


Parameter		mean μ	standard deviation σ
Sinusoidal length	L_{sin}	500 μm	70 μm
Sinusoidal radius	y_{sin}	4.4 μm	0.45 μm
Width of Disse space	y_{dis}	0.8 μm	0.3 μm
Hepatocyte sheet thickness	y_{cell}	1/4 * 25 μm	1/4 * 5 μm
Blood flow velocity	v_{RBC}	60 μm/s	50 μm/s

- whole liver modelled by integrating heterogeneous contribution of sinusoidal units differing in blood-flow and tissue-architecture



WORK IN PROGRESS



- Calculation of distributions of sinusoidal units
 - optimized C++ integration routines
 - parallelization & integration
- Simulations of alterations
 - **Galactosemias**
 - **homogeneous**
 - changes in GEC during aging
 - changes in GEC during CCL4 intoxication
 - changes in GEC during
 - **heterogeneous**
 - local perfusion inhomogeneities

WORK IN PROGRESS

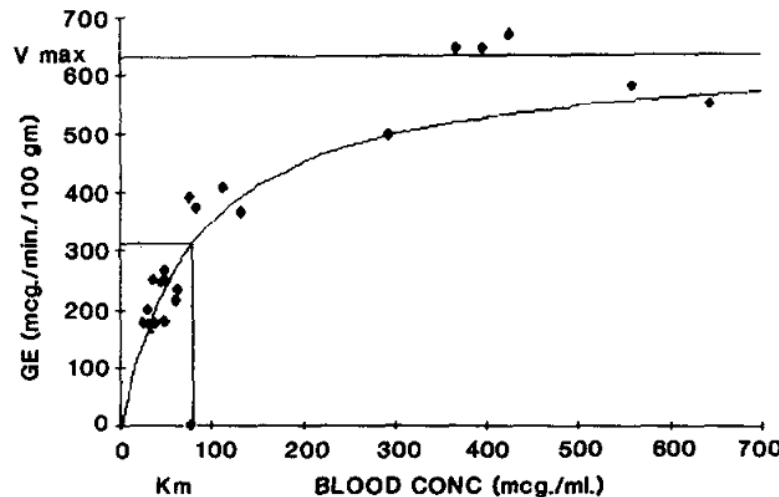


FIG. 1. Galactose elimination kinetics. Points represent individual animals. Superimposed line as determined by the Michaelis-Menten equation using the elimination constants, V_{\max} and K_m , from Fig. 2.

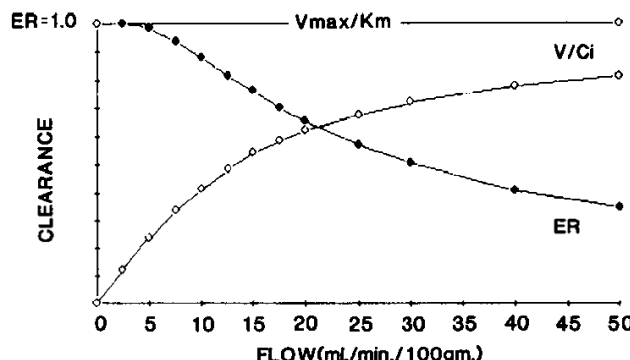
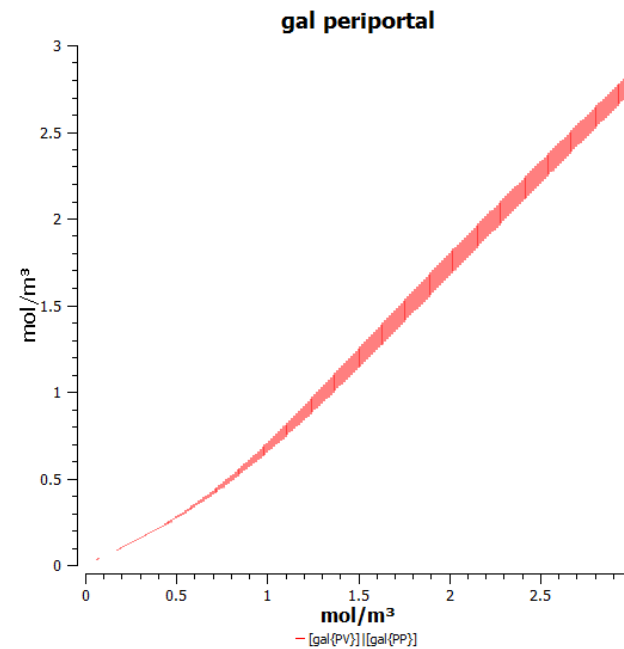


FIG. 6. Clearance and extraction ratio vs flow. Extraction ratio decreases as flow increases. Clearance increases with flow to a maximum of V_{\max}/K_m .



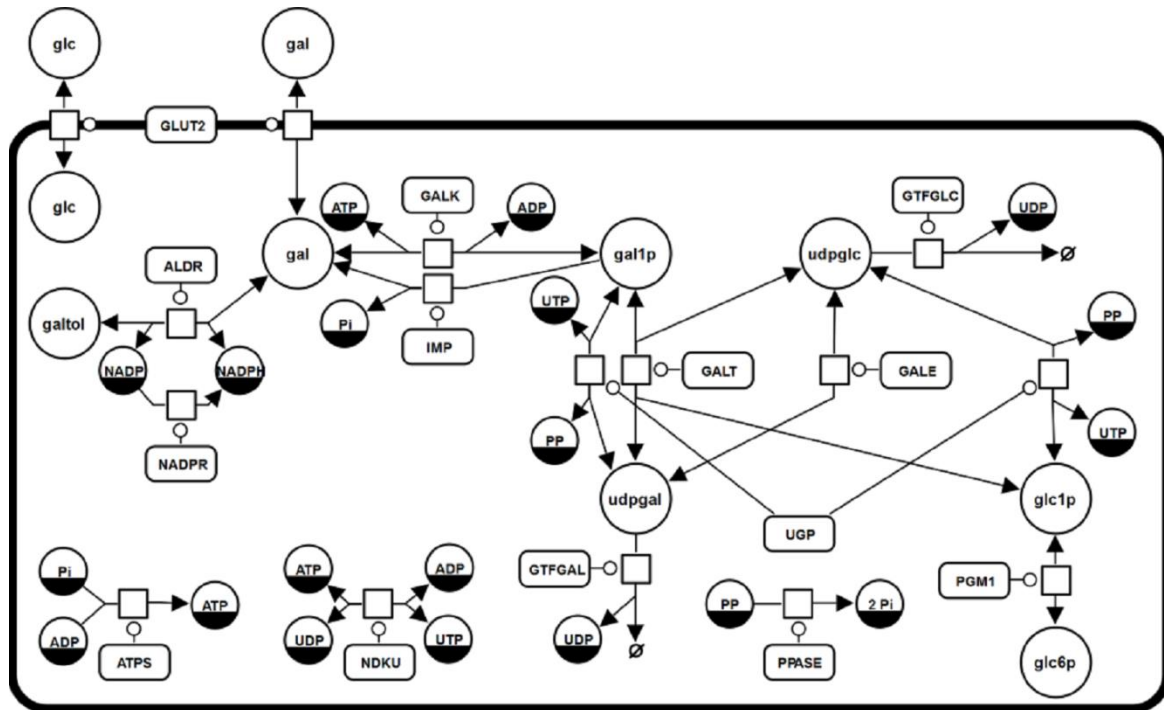
TODO: Improving Integration Times

- generation of optimized C++ code for solver

CELLULAR SCALE - HEPATOCYTES

GALACTOSE METABOLISM

- liver most important organ for whole-body metabolism and clearance of galactose
- Main enzymatic steps
 - I. **Galactokinase (GALK)** phosphorylation of galactose (gal) to galactose 1-phosphate (gal1p) catalysed
 - II. **Galactose-1-phosphate uridyl transferase (GALT)** conversion of gal1p to UDP-galactose (udpgal)
 - III. **UDP-galactose 4'-epimerase (GALE)** interconversion of udpgal and UDP-glucose (udpglc)
- Galactose can enter glycolysis as glucose-1 phosphate (glc1p)
- Galactose can be incorporated in glycoproteins and glycolipids as udpgal



Reactions: (ALDR) Aldose reductase (galactitol NAD 1-oxidoreductase); (ATPS) ATP synthesis; (GALDH) Galactose 1-dehydrogenase; (GALE) UDP-glucose 4-epimerase; (GALK) Galactokinase; (GALT) Galactose-1-phosphate uridyl transferase; (GLUT2) Facilitated glucose transporter member 2; (GTFGAL) Glycosyltransferase galactose; (GTFGLC) Glycosyltransferase glucose; (NADPR) NADP reductase; (NDKU) Nucleoside diphosphokinase, ATP:UDP phosphotransferase; (IMP) Inositol monophosphatase; (PGM1) Phosphoglucomutase-1; (PPASE) Pyrophosphatase; (UGALP) UDP-galactose pyrophosphorylase; (UGP) UDP-glucose pyrophosphorylase;
 Metabolites: (adp) ADP; (atp) ATP; (gal) D-galactose; (gal1p) D-galactose 1-phosphate; (galnat) D-galactonate; (galtol) D-galactitol; (glc) D-glucose; (glc1p) D-glucose 1-phosphate; (glc6p) D-glucose 6-phosphate; (nadp) NADP; (nadph) NADPH; (pi) phosphate; (pp) pyrophosphate; (udp) UDP; (udpgal) UDP-D-galactose; (udpglc) UDP-D-glucose; (utp) UTP;

GALACTOSEMIAS

Table 4 - Kinetic parameters in GALK, GALT and GALE deficiencies.

- caused by **deficiencies in either GALK, GALT or GALE**
- untreated as well as treated patients with galactosemia show accumulation and/or depletion of specific metabolites, and often abnormalities of glycosylation

implementation

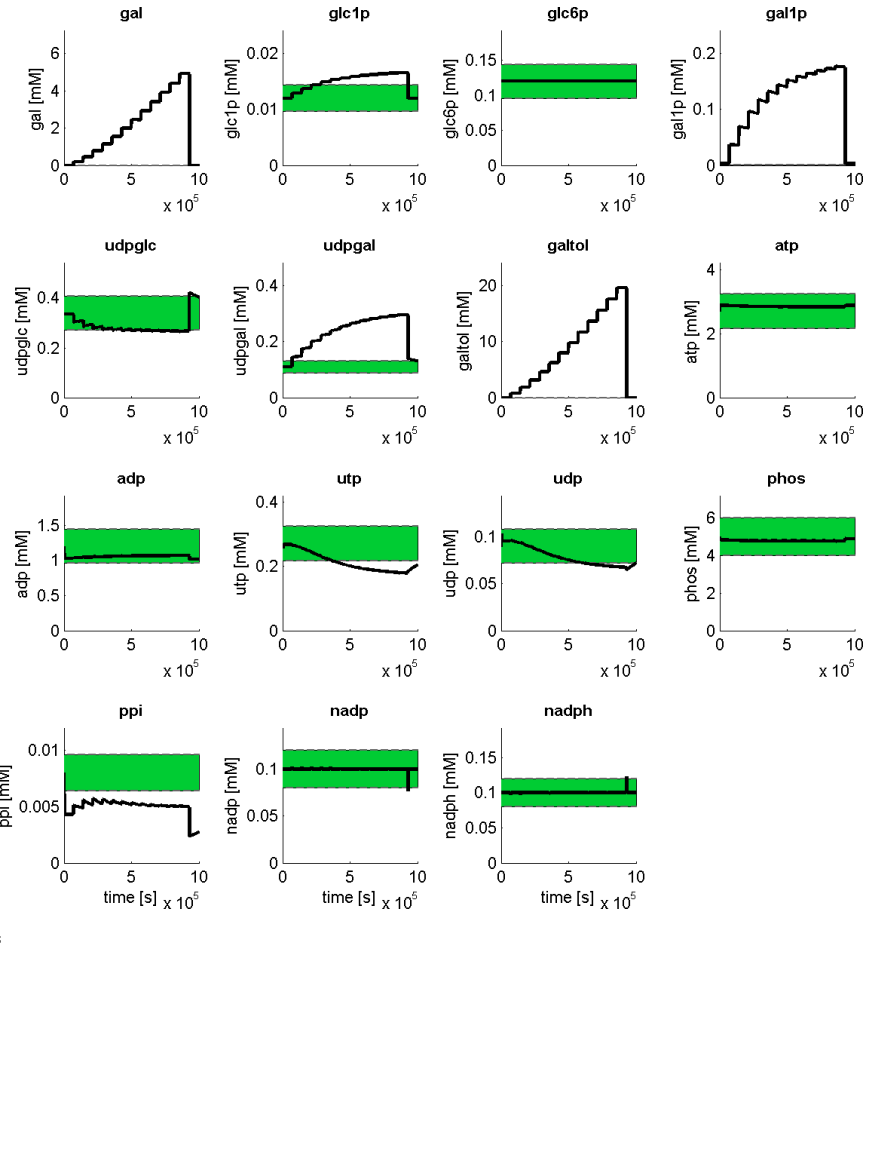
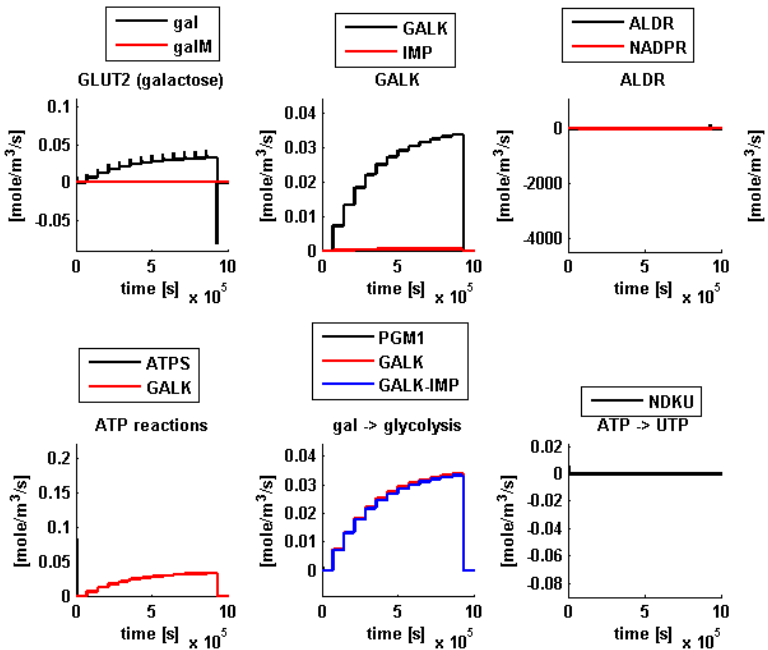
- via measured alterations in kinetic properties in human protein mutations

Enzyme	Variant	k_{cat} [1/s] (%wt)	$K_m(\text{gal})$ [mM] (%wt)	$K_m(\text{atp})$ [mM] (%wt)	Reference
GALK	Wild Type	8.7±0.5 (100)	0.97±0.22 (100)	0.034±0.004 (100)	[51]
1	GALK H44Y	2.0±0.1 (23)	7.70±4.40 (794)	0.130±0.009 (382)	[51]
2	GALK R68C	3.9±0.8 (45)	0.43±0.15 (44)	0.110±0.035 (324)	[51]
3	GALK A198V	5.9±0.1 (68)	0.66±0.22 (68)	0.026±0.001 (76)	[51]
4	GALK G346S	0.4±0.04 (5)	1.10±0.16 (113)	0.005±0.002 (15)	[51]
5	GALK G347S	1.1±0.2 (13)	13.0±2.0 (1340)	0.089±0.034 (262)	[51]
6	GALK G349S	1.8±0.1 (21)	1.70±0.48 (175)	0.039±0.004 (115)	[51]
7	GALK E43A	6.7±0.02 (77)	1.90±0.50 (196)	0.035±0.0003 (103)	[100]
8	GALK E43G	0.9±0.02 (10)	0.14±0.01 (14)	0.0039±0.0006 (11)	[100]
Enzyme	Variant	V_{max} [nmol/mg/s] (% wt)	$K_m(\text{gal1p})$ [mM] (%wt)	$K_m(\text{udpglc})$ [mM] (%wt)	Reference
GALT	Wild Type	804±65 (100)	1.25±0.36 (100)	0.43±0.09 (100)	[22]
9	GALT R201C	396±59 (49)	1.89±0.62 (151)	0.58±0.13 (135)	[22]
10	GALT E220K	253±53 (31)	2.34±0.42 (187)	0.69±0.16 (160)	[22]
11	GALT R223S	297±25 (37)	1.12±0.31 (90)	0.76±0.09 (177)	[22]
12	GALT I278N	45±3 (6)	1.98±0.35 (158)	1.23±0.28 (286)	[22]
13	GALT L289F	306±23 (38)	2.14±0.21 (171)	0.48±0.13 (112)	[22]
14	GALT E291V	385±18 (48)	2.68±0.16 (214)	0.95±0.43 (221)	[22]
Enzyme	Variant	k_{cat} [1/s] (%wt)	$K_m(\text{udpglc})$ [mM] (%wt)	Reference	
GALE	Wild Type	36±1.4 (100)	0.069±0.012 (100)	[59]	
15	GALE N34S	32±1.3 (89)	0.082±0.015 (119)	[59]	
16	GALE G90E	0.046±0.0028 (0)	0.093±0.024 (135)	[59]	
17	GALE V94M	1.1±0.088 (3)	0.160±0.038 (232)	[59]	
18	GALE D103G	5.0±0.23 (14)	0.140±0.021 (203)	[59]	
19	GALE L183P	11±1.2 (31)	0.097±0.040 (141)	[59]	
20	GALE K257R	5.1±0.29 (14)	0.066±0.015 (96)	[59]	
21	GALE L313M	5.8±0.36 (16)	0.035±0.011 (51)	[59]	
22	GALE G319E	30±1.3 (83)	0.078±0.013 (113)	[59]	
23	GALE R335H	15±0.48 (42)	0.099±0.012 (143)	[59]	

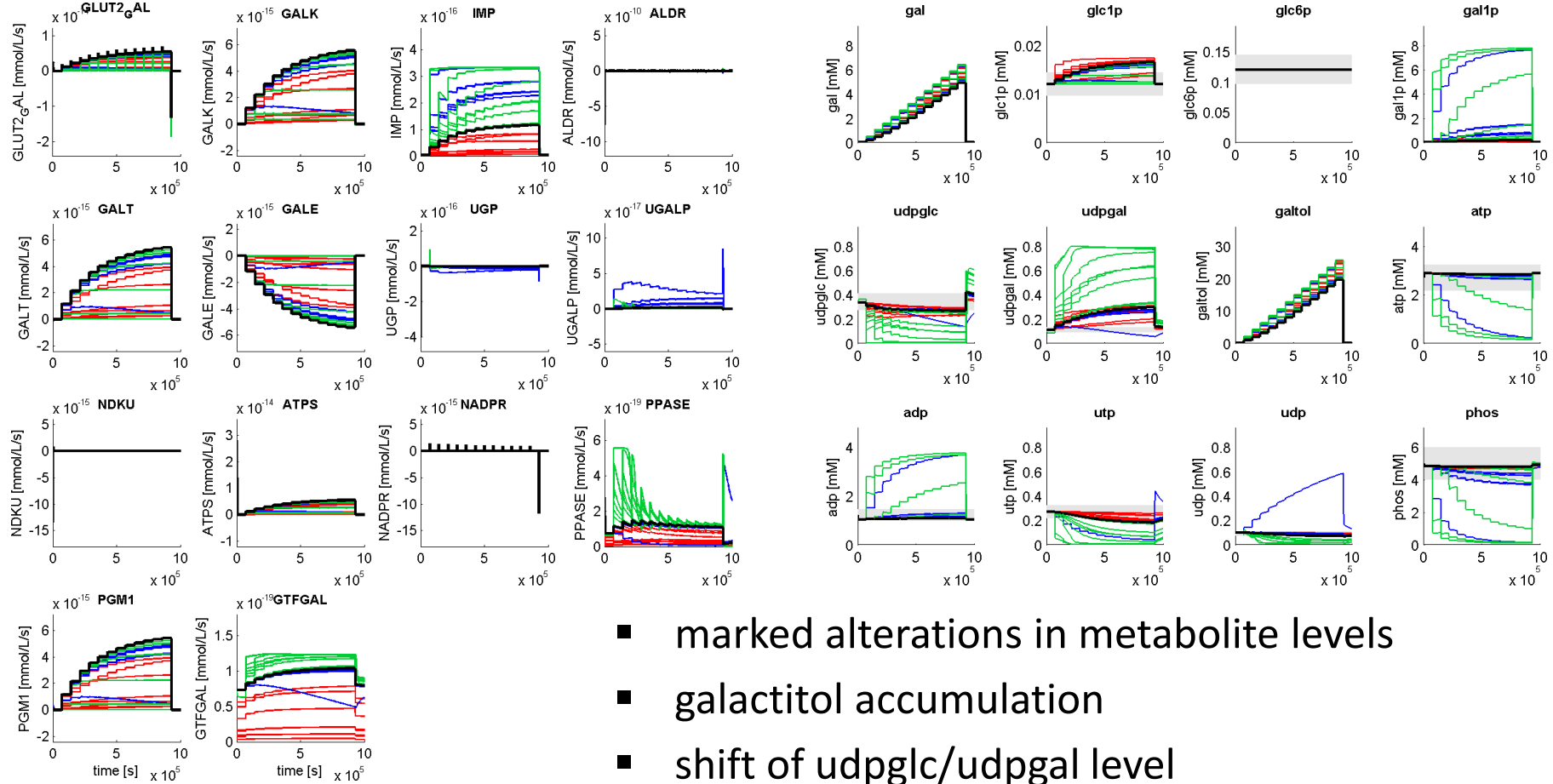
HEPATOCYTE MODEL

- Reproduces

- metabolic concentrations normal state
- altered metabolite levels during galactose challenge
- saturation of clearance capacity



GALACTOSEMIA (GALK, GALT, GALE)



- marked alterations in metabolite levels
- galactitol accumulation
- shift of udpglc/udpgal level
- reduced galactose clearance
- energetically challenged

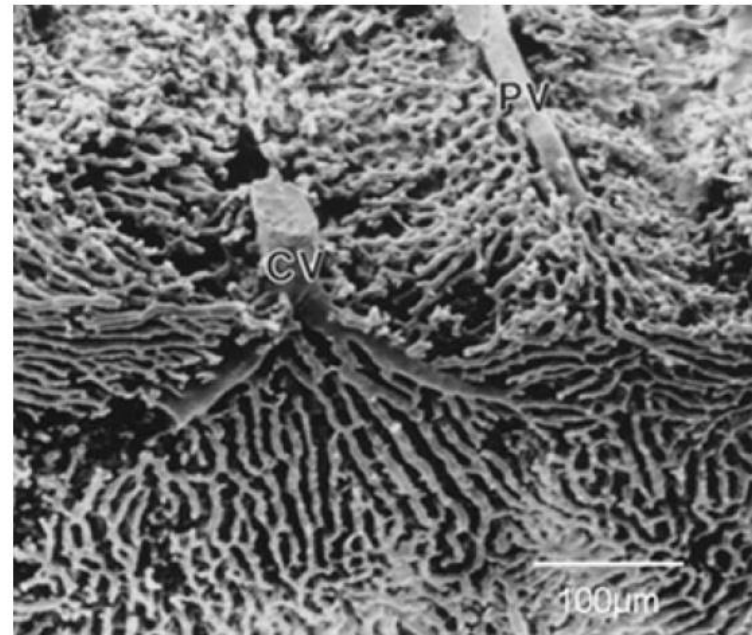
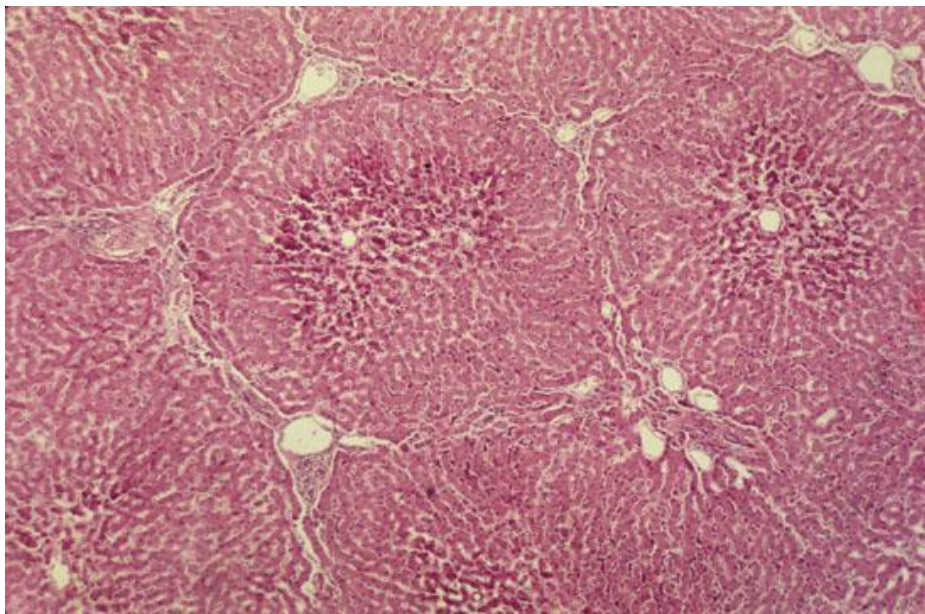


Fig. 2. Vascular cast of the hepatic microvasculature illustrating the tortuous, anastomotic sinusoids adjacent to the portal venule (PV) and the more parallel and larger sinusoids near the central venule (CV) (McCuskey, 1993).

SINUSOID

- principal vessels for exchange between blood and hepatocytes
- ~ 6-8 μm diameter
- periportal sinusoids are narrower and more tortuous than the wider and straighter central ones
- Sinusoid network is heterogeneous
 - near portal vein arranged as interconnecting polygonal networks
 - farther away from portal vein organized as parallel vessels terminating in the central vein
 - short intersinusoidal sinusoids connect adjacent parallel sinusoids

Scanning electron micrograph showing fenestrated sinusoids and hepatocytes in a mouse liver.

http://www.easloffice.eu/jhep/contest/website/see_photos.html

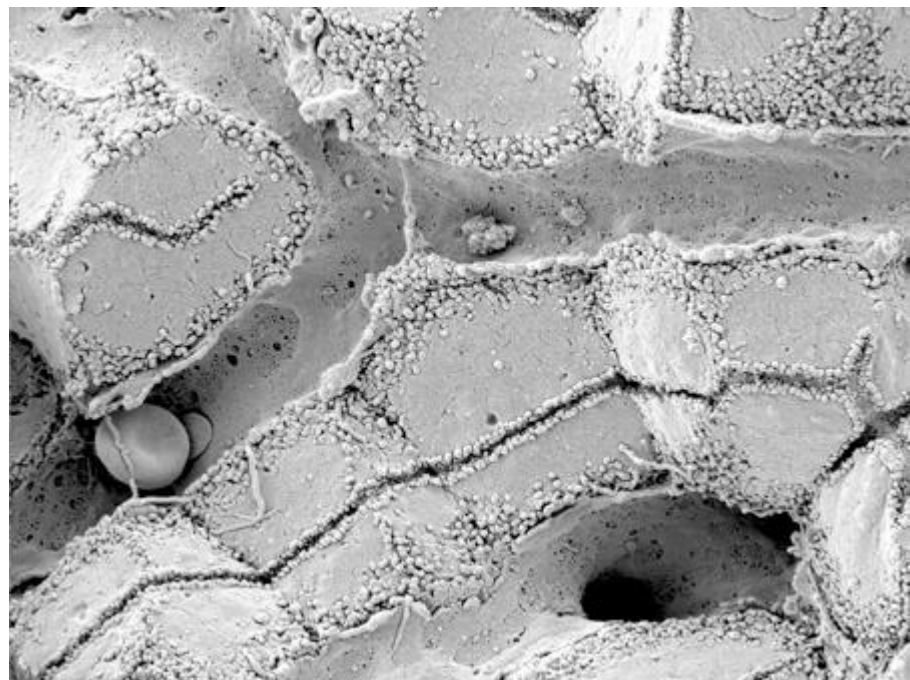


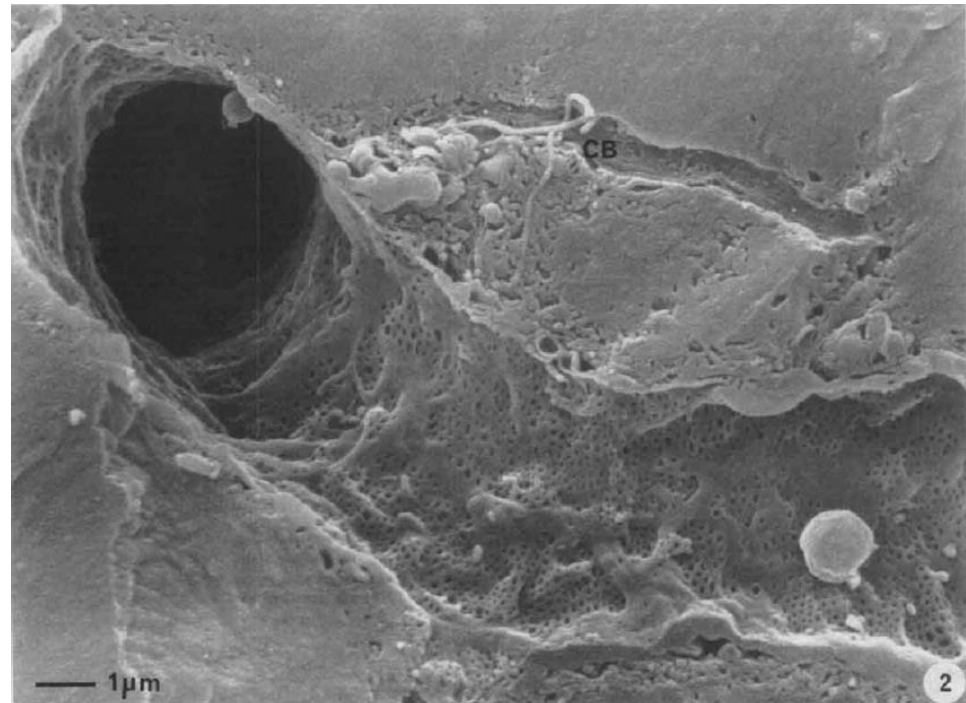
TABLE 1. COMPARISON OF MEASUREMENTS ON SINUSOIDS AND BLOOD CELLS IN MICRONS \pm S.E.

	In vivo/LM ^a	In plastic/LM	After CPD/SEM
Portal sinusoid	5.9 ± 0.17 (n = 545, 6 rats)	6.42 ± 0.12 (n = 696, 2 rats)	4.09 ± 0.06 (n = 1, 452, 10 rats)
Central sinusoid	7.1 ± 0.29 (n = 498, 6 rats)	$7.62 \pm \text{ND}^b$ (n = 696, 2 rats)	$5.67 \pm \text{ND}$ (n = 1, 452, 10 rats)

Scanning electron microscope observations on the structure of portal veins, sinusoids and central veins in rat liver. Wisse, E.; De Zanger, R. B.; Jacobs, R. & McCuskey, R. S.; *Scan Electron Microsc*, 1983, 1441-1452
The liver sieve: considerations concerning the structure and function of endothelial fenestrae, the sinusoidal wall and the space of Disse. Wisse, E.; De Zanger, R. B.; Charels, K.; Van Der Smissen, P. & McCuskey, R. S. *Hepatology*, 1985, 5, 683-692

ENDOTHELIAL FENESTRAE

- liver sinusoids unique capillaries
 - **open pores (fenestrae)** in sinusoidal wall
 - **lack basal membrane** underneath endothelium
- fenestrae act as sieving barrier between blood and hepatocytes
 - morphological & physiological evidence that fenestrae act as a **dynamic filter**
 - important role in lipid metabolism (namely **chylomycrons**)
- Liver sinusoidal endothelial cells (**LSEC**) constitute sinusoidal wall
 - numerous endocytotic vesicles
 - effective uptake of a wide variety of substances from blood via receptor-mediated endocytosis (Braet, 2004)
 - transcytosis transport across the endothelium to surrounding tissue
 - scavenger system



Contribution of high-resolution correlative imaging techniques in the study of the liver sieve in three-dimensions. Braet, F. et al; *Microsc Res Tech*, 2007, 70, 230-242
Structural and functional aspects of liver sinusoidal endothelial cell fenestrae: a review. *Comp Hepatol*, Braet, F. & Wisse, E., 2002, 1, 1
The liver sieve: considerations concerning the structure and function of endothelial fenestrae, the sinusoidal wall and the space of Disse. Wisse, E.; De Zanger, R. B.; Charels, K.; Van Der Smissen, P. & McCuskey, R. S. *Hepatology*, 1985, 5, 683-692

FENESTRAE

- diameter ~**50-200nm**
- ultrastructure same across species
 - groups of fenestrae arranged in so called **sieve plates**
- differences periportal & perivenous
 - diameter decreases (110.7 to 104.8nm)
 - frequency increases (9 to 13 per μm^2)
 - increased porosity from pp to pv from 6 to 8%
- number and diameter may vary between individuals & within single individual under various physiological and pharmacological circumstances

Scanning electron micrograph of hepatocyte microvilli protruding through the sinusoidal endothelial cell fenestrations.

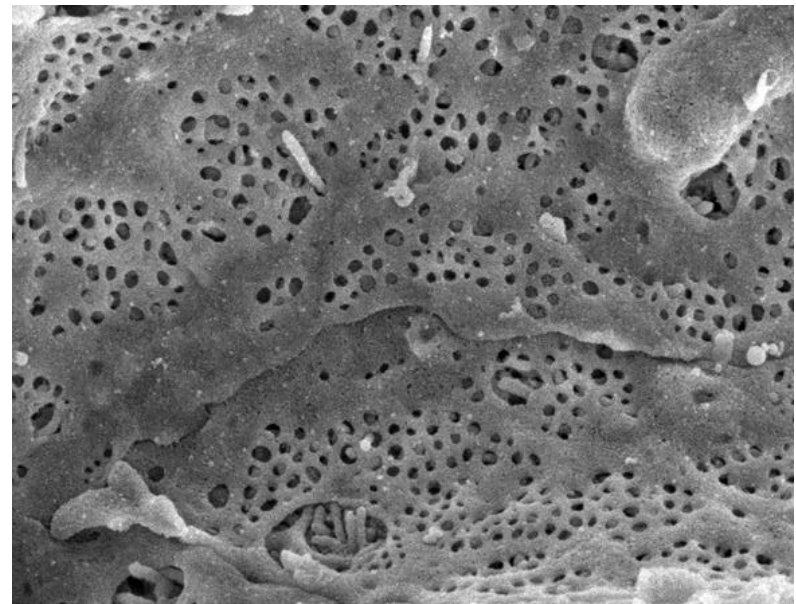
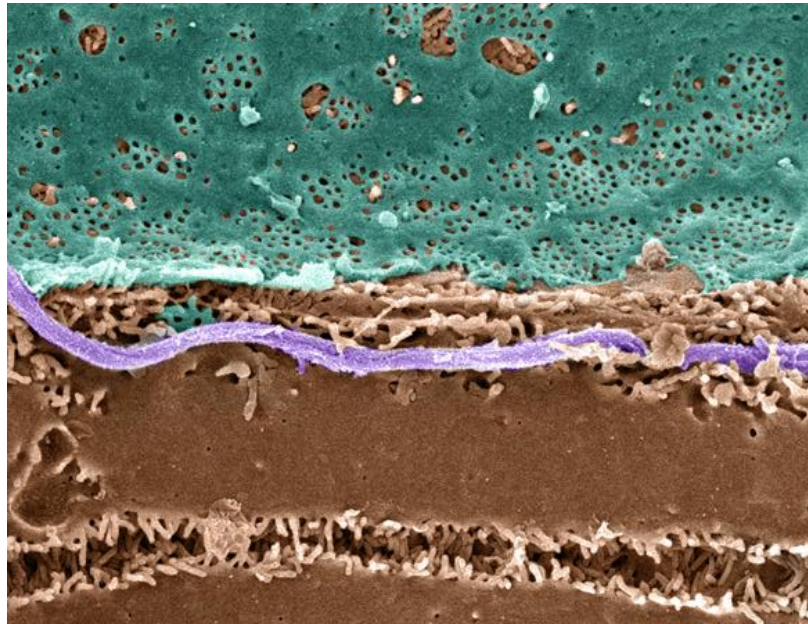


Table I: Fenestration pattern in different species Brief overview of fenestrae characteristics of different species. Notice the large variations in diameter and number of fenestrae between the different species. The reported data from this table were obtained by at random measurements along the sinusoids. "n.d." = no data available. Data are expressed as mean \pm S.D. In case of baboon, human and rainbow trout the data correspond with the minimum and maximum diameter or number of fenestrae measured.

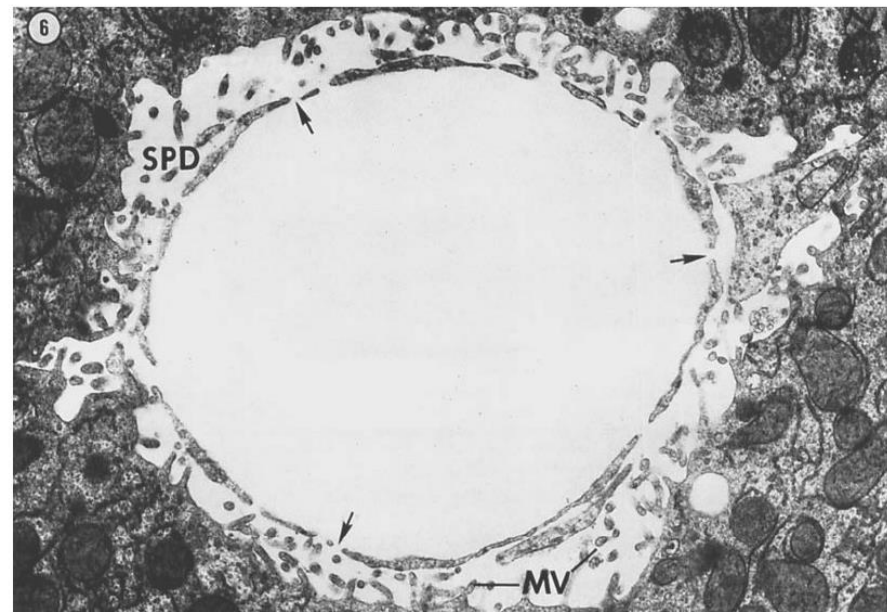
Species (ref.)	Diameter (nm)	Number of fenestrae / μm^2
Rat [25]	98.0 ± 13.0	20.0 ± 6.3
Mouse [26]	99.0 ± 18.0	14.0 ± 5.0
Rabbit [27]	59.4 ± 4.8	17.3 ± 3.8
Chicken [23]	89.6 ± 17.8	2.9 ± 0.3
Baboon [20]	92 – 116	1.4 – 1.9
Human [28]	50 – 300	15 – 25

SPACE OF DISSÉ



Pseudo-colored Scanning EM of an hepatic plate,
accentuating the **fenestrated
sinuoidal endothelium (blue)**, **hepatocyte
(brown)** and a **collagen fibril (lavender)**.

Hepatocytes surface enlarged via **microvilli**.



6 Intermediate sinusoid. The lining cells possess fenestrations (arrows) and there is no basement membrane. The space of Dissé (SPD) is voluminous. The surface of the parenchymal cells is characterized by numerous microvillae (MV). The blood plasma has free access to the liver cells. Glutaraldehyde; OsO₄; Epon; 13,500 ×.

SINUSOID ULTRASTRUCTURE

- fenestraetion & absence of basement membranes provide direct access of blood plasma to hepatocytes

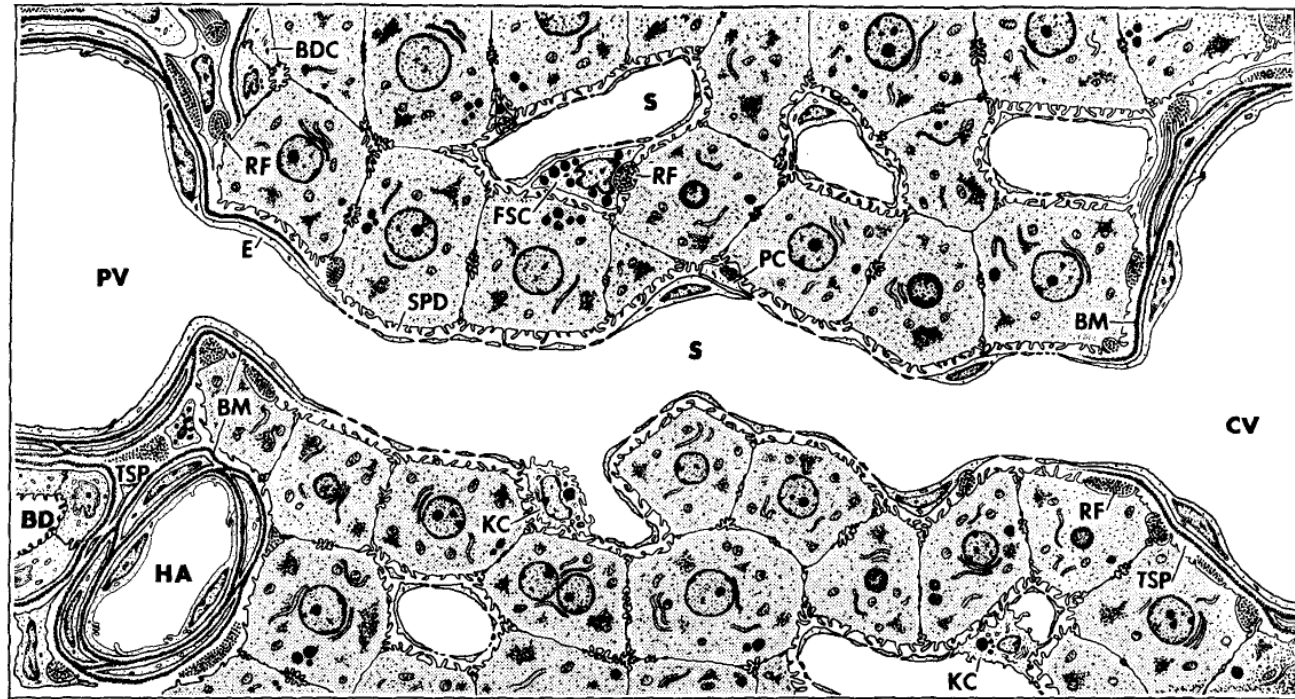


Fig. 1 Fine structure in the rat liver lobule. The periphery of the lobule is at the left where branches of portal vein (PV) hepatic artery (HA) and bile duct (BD) lie in the tissue space (TSP). Above, bile duct cells (BDC) abut on liver cells. The sinusoid (S) connects the portal vein with the central vein (CV). In the peripheral portion of the sinusoid both the endothelium (E) and its basement (boundary) membrane (BM) are continuous with those of the portal vein. In the intermediate portion the lining is fenestrated and there is no basement membrane. Centrally the cellular lining is continuous with the endothelium of the central vein and a basement membrane is present. Reticular fibers (RF) are found in the tissue space and in the space of Dissé (SPD) which surrounds the sinusoids. In places the sinusoids are lined by the cells of von Kupffer (KC). Perisinusoidal cells (PC) and fat storage cells (FSC) are in the space of Dissé. See text for interpretation.

TIGHT SINUSOIDS

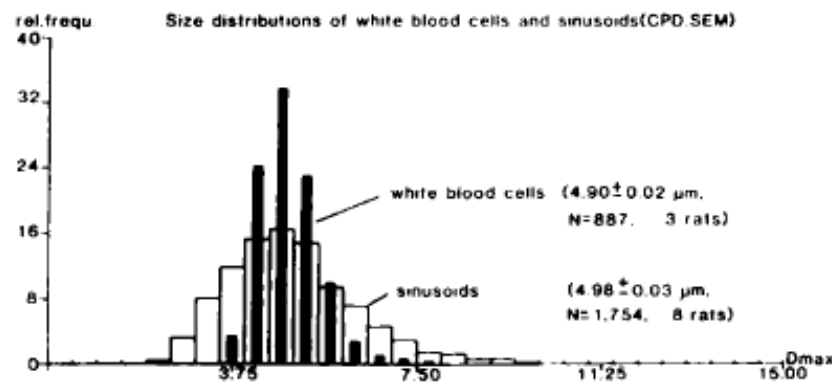
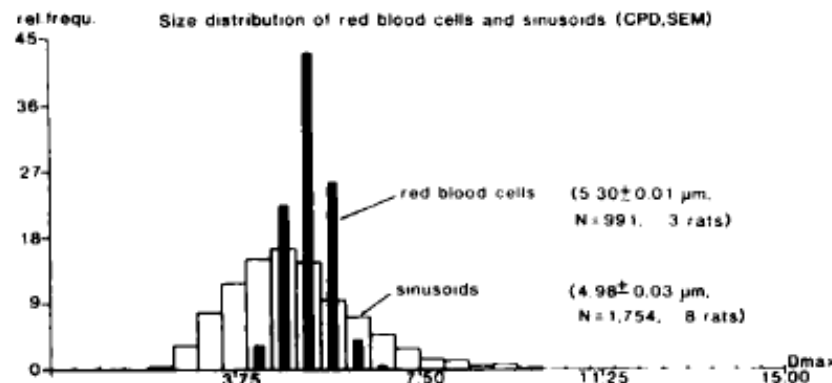


FIG. 9. Size distribution of sinusoids and red and white blood cells, extending the data of Table 1. From these two graphs, one might conclude that starting at 3.75 μm blood cells are larger than a certain percentage of sinusoids. At about the size of 7 μm , white blood cells are bigger than most sinusoids, and these cells will progressively plug sinusoids in the range of approximately 4 μm (in SEM preparations).

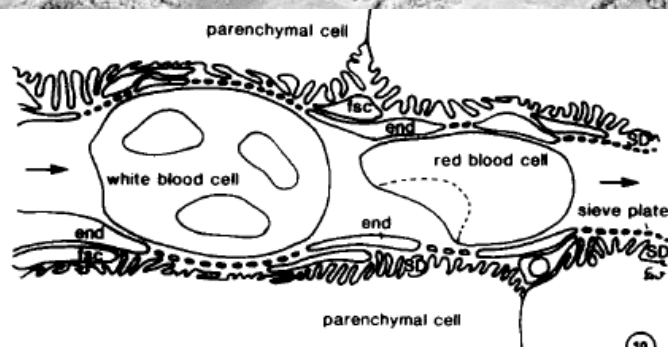
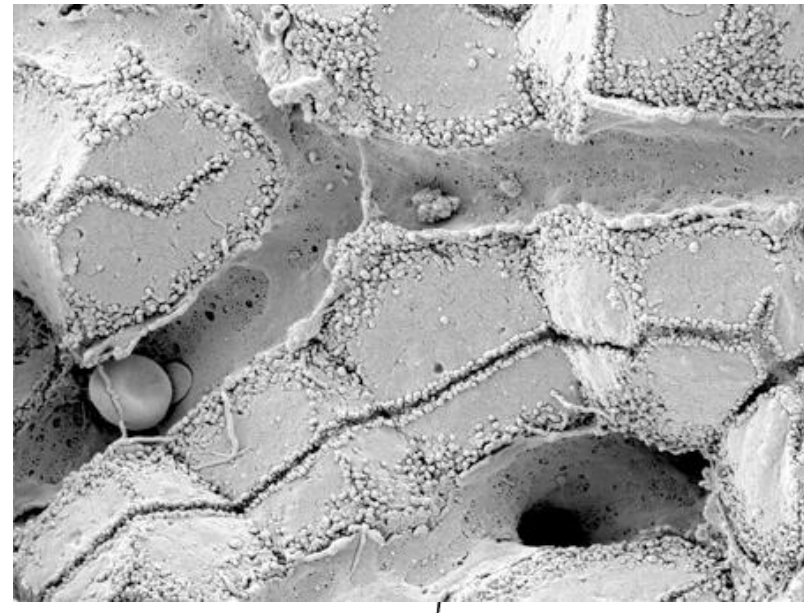


FIG. 10. shows the interaction of blood cells and the fenestrated sinusoidal wall. As observed in the *in vivo* microscope, red blood cells pass by in a single row and show typical deformation morphology. Their observed flexibility is enormous, and in slow streaming sinusoids one observes that red blood cells adapt their diameter constantly to the diameter of the sinusoid by expanding and narrowing. This implies that uptake and exchange is taking place from volumes of plasma in between the red blood cells. White blood cells are much more rigid than red blood cells and are thought to compress the space of Disse, thereby performing endothelial massage (Fig. 12).

BLOOD FLOW

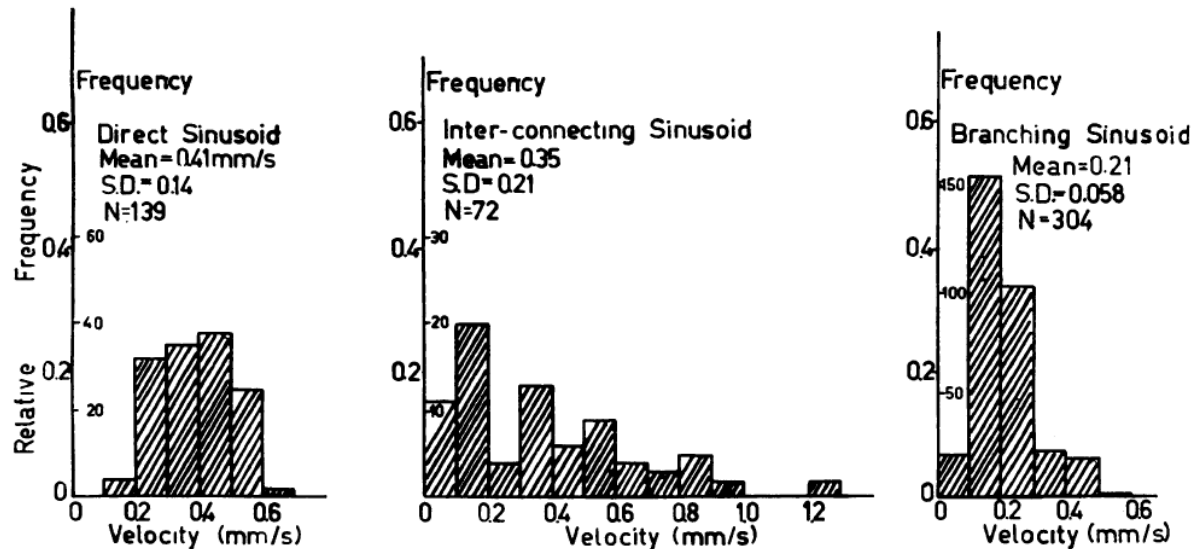


FIG. 1. Frequency distribution of the velocity of the erythrocytes in the direct sinusoids, the branching sinusoids and the interconnecting sinusoids.

The terminal hepatic microcirculation in the rat.

Koo, A.; Liang, I. Y. & Cheng, K. K.; *Q J Exp Physiol Cogn Med Sci*, 1975, 60, 261-266

Intermittence of blood flow in liver sinusoids, studied by high-resolution *in vivo* microscopy. MacPhee, P. J.; Schmidt, E. E. & Groom, A. C.; 1995, 269, G692-G698

BLOOD FLOW

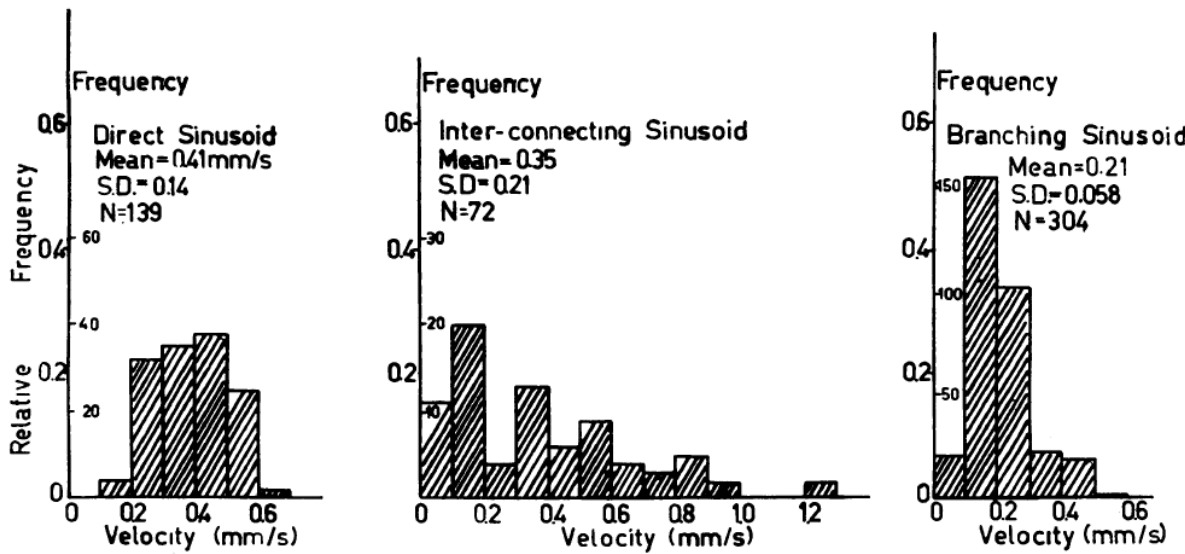
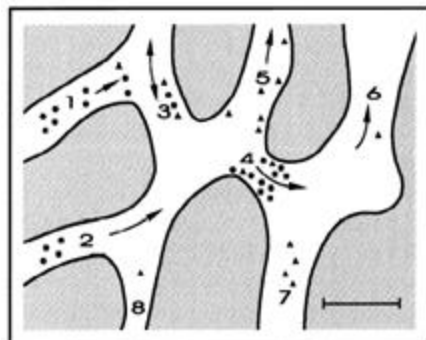


FIG. 1. Frequency distribution of the velocity of the erythrocytes in the direct sinusoids, the branching sinusoids and the interconnecting sinusoids.



The terminal hepatic microcirculation in the rat.

Koo, A.; Liang, I. Y. & Cheng, K. K.; *Q J Exp Physiol Cogn Med Sci*, 1975, 60, 261-266

Intermittence of blood flow in liver sinusoids, studied by high-resolution *in vivo* microscopy. MacPhee, P. J.; Schmidt, E. E. & Groom, A. C.; 1995, 269, G692-G698

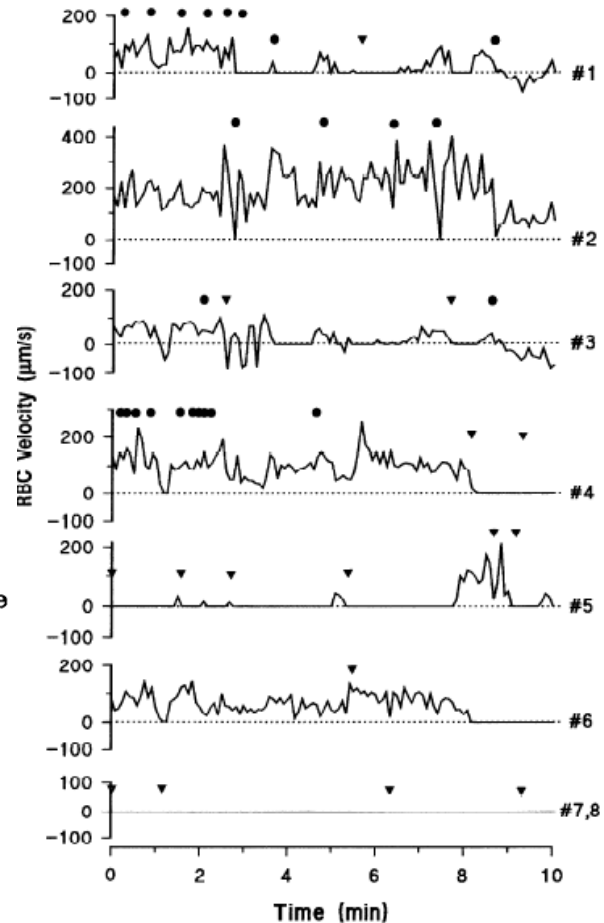


Fig. 3. Temporal overview of RBC velocity fluctuations over a 10-min period, in sinusoidal network from zone 1 of mouse liver (shown in Fig. 2). Measurements in each sinusoid were made every 5 s. Changes of flow in one sinusoid often produced changes in others. Instants are indicated at which a migrating Kupffer cell obstructed flow (▼) or a circulating leukocyte slowed or stopped temporarily (●). Sinusoids 7 and 8 had no flow throughout the 10-min period. Kupffer cells are seen in sinusoid 7, and in sinusoid 8 one Kupffer cell blocked flow throughout.

LYMPH

- substantial amount of hepatic lymph is generated in space of Dissé
 - space of Dissé is continuous with the tissue space at both ends of the sinusoid !
 - high protein content of hepatic lymph
- **lymphatic vessels** originate as blind-ending capillaries in the connective tissue spaces (portal tracts) associated with the portal veins and hepatic arteries
 - fluid contained in these lymphatics flows toward the **hepatic hilus** and eventually into the **cisternae chyli**

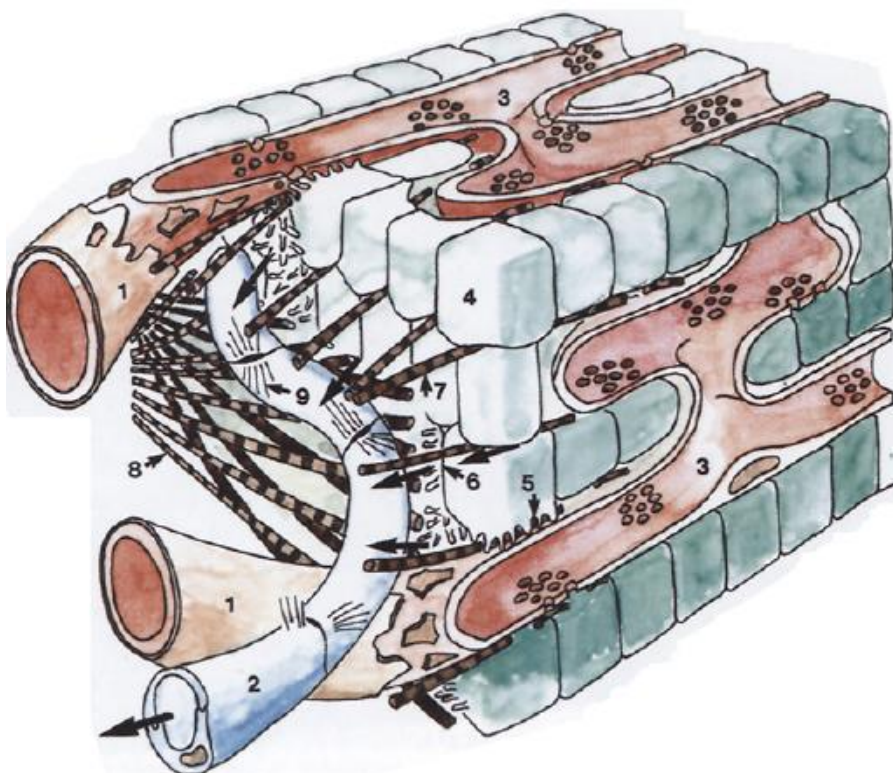


Fig. 5. Terminal lymphatics of the periportal area. The *thick arrows* indicate the possible lymph flow, coming from the space of Dissé and entering a terminal lymphatic. The continuity between the space of Dissé and the periportal area is represented by collagen fibers. 1, blood capillary entering the liver parenchyma; 2, terminal lymph vessel; 3, sinusoid; 4, periportal hepatocyte; 5, space of Dissé; 6, space of Mall; 7, collagen fibers entering the limiting plate; 8, network of periportal collagen fibers; 9, anchoring filaments

Lymph circulation in the liver.

Ohtani, O. & Ohtani, Y.; *Anat Rec*; 2008, 291, 643-652

The lymphatics of the liver.

Trutmann, M. & Sasse, D.; *Anat Embryol (Berl)*, 1994, 190, 201-209